New particle formation in the active volcanic plume of the Piton de la Fournaise: specific features from a long-term dataset

Clémence Rose[1], Brice Foucart[2], David Picard[1], Aurélie Colomb[1], Jean-Marc Metzger[3], Pierre Tulet[2], Karine Sellegri[1]

[1]Laboratoire de Météorologie Physique (LaMP-UMR 6016, CNRS, Université Clermont Auvergne), 63178, Aubière, France.
[2]Laboratoire de l'Atmosphère et des Cyclones (LACy-UMR 8015, CNRS, Université de La Réunion, Météo France), 97744 Saint Denis de La Réunion, France.
[3]Observatoire des Sciences de l'Univers de La Réunion, UMS 3365 (CNRS, Université de La Réunion), 97744, Saint Denis de La Réunion, France.

Correspondence to: Clémence Rose (c.rose@opgc.univ-bpclermont.fr) and Karine Sellegri (k.sellegri@opgc.univ-bpclermont.fr)

Abstract

New particle formation (NPF) is a key atmospheric process which may be responsible for a major fraction of the total aerosol number burden at the global scale, including in particular cloud condensation nuclei (CCN). NPF has been observed in various environments around the world, but some specific conditions, such as those encountered in volcanic plumes, remain poorly documented in the literature. Yet, understanding such natural processes is essential to better define preindustrial conditions in climate model simulations, as those form the baseline to calculate the radiative forcing caused by anthropogenic emissions. Here we report observations of NPF performed at the high-altitude observatory of Maïdo (2165 m a.s.l., La Réunion Island) between 1st January and 31st December 2015. During this time period, 3 effusive eruptions of the Piton de la Fournaise, located ~ 39 km away from the station, were observed and documented, resulting in 36 days of measurement in volcanic plume conditions to be compared with 250 "non-plume days". This dataset is, to our knowledge, the largest ever reported for the investigation of NPF in tropospheric volcanic plume conditions, and allowed for the first time a statistical approach to characterize the process and also assess its relevance with respect to non-plume conditions. NPF was observed on 86% of the plume days vs 71% of the non-plume days during the 4 months when the eruptions occurred. The events were on average detected earlier on plume days, most likely benefiting from larger amounts of precursors available at the site prior to nucleation hours compared to non-plume days, during which condensable species were in contrast transported from lower altitude by the mean of convective processes. Surprisingly, the overall effect of the plume conditions on the particle growth rate was limited. However, with the exception of September, particle formation rates were significantly higher on plume days. The signature of the volcanic plume on the aerosol spectra up to $d_P = 600$ nm was further investigated based on the analysis and fitting of the particle size distributions recorded in the different conditions. The spectra recorded prior to nucleation hours, in absence of freshly formed particles, featured a significant contribution of particles likely formed *via* heterogeneous processes at the vent of the volcano (and assimilated to volcanic primary particles) to the concentrations of the 2 accumulation modes on plume days. Later on in the morning, the concentrations of the nucleation and Aitken modes showed important variations on plume

days compared to event days outside of plume conditions. The spectra recorded on event days, in and off-plume conditions, were further used to provide an average size distribution of the particles of volcanic origin, which clearly highlighted the dominant contribution of secondary over primary particles (96%) to the total concentration measured on NPF event days within volcanic plume. In a next step, particular attention was paid to the concentration of particles with $d_p > 50$ nm (N_{50}), used as a

5   proxy for potential CCN population. The contribution of secondary particles to the increase of N_{50} was the most frequent in plume conditions, and the magnitude of the increase was also more important on plume days compared to non-plume days. Last, in order to further evaluate the effect of volcanic plume conditions on the occurrence of NPF, we analysed the variations of the condensation sink (CS) and [H_2SO_4], previously reported to play a key role in the process. Over the investigated months, higher CS (calculated prior to nucleation hours) were observed in plume conditions, and coincided with high SO_2 mixing

10 ratios. Those most likely compensated for the strengthened loss rate of the vapour and favoured the occurrence of NPF, suggesting at the same time a key role of H_2SO_4 in the process. This last hypothesis was further supported by the correlation between the formation rate of 2 nm particles (J_2) and [H_2SO_4], and by the fair approximation of J_2 that was obtained by the mean of a recent parameterisation of the binary nucleation of $H_2SO_4 - H_2O$. This last result was of high interest as it also demonstrated that in absence of direct measurement of [H_2SO_4] and sub-2nm particles concentration, estimates of J_2 could be

15 obtained from the knowledge of SO_2 mixing ratios only.

1 Introduction

Aerosol particles are a complex component of the atmospheric system which affects both air quality and climate. They have been the focus of a growing number of studies during the last decades, but our knowledge of their sources, properties, including their ability to interact with other atmospheric components and associated effects on the Earth's climate system, remains

20 nonetheless uncomplete. In specific, while particles are known to affect the formation of clouds, and in turn their properties (Albrecht, 1989; Rosenfeld et al., 2014), the radiative forcing associated to these effects (usually referred to as "indirect effect") still has a large uncertainty (Myhre et al., 2013). Better understanding and quantification of this indirect effect requires, in particular, more accurate information on secondary aerosol particle sources, and in turn on new particle formation (NPF). Indeed, measurements conducted in various environments suggest that NPF might be an important source of cloud

25 condensation nuclei (CCN) (e.g. Kerminen et al., 2012; Rose et al., 2017), which is further supported by model investigations (Merikanto et al., 2009; Makkonen et al., 2012; Gordon et al., 2017). However, despite significant improvement of instrumental techniques for the characterisation of the newly formed particles and their precursors (Junninen et al., 2010; Vanhanen et al., 2011; Jokinen et al., 2012), model predictions are still affected by our limited understanding of NPF. In addition, the scarcity of observations makes it all the more uncertain in hard-to-reach environments, or in specific conditions, such as those

30 encountered in volcanic plumes.

Volcanic eruptions are one of the most important natural sources of some specific gases and aerosol particles in the atmosphere. A variety of gaseous species have been identified in volcanic plumes, among which halogens (Aiuppa et al., 2009; Mather,

2015) and sulfur dioxide (SO_2), which can be further oxidized to sulfuric acid (H_2SO_4). SO_2 is released in significant amount, in particular during eruptive periods but also from passive degassing (Andres and Kasgnoc, 1998; Robock, 2000; Tulet et al., 2017), and it was reported that all together, volcanoes contribute significantly to the global sulfur budget, which is otherwise dominated by anthropogenic sources (Penner et al., 2001 and references therein; Seinfield and Pandis, 2006). Volcanic aerosols

5   are injected in the atmosphere both as primary or secondary particles. The former are fragments of ash which, despite their relatively large sizes (up to few microns) (Robock, 2000), can be transported over long distances in the atmosphere (Hervo et al., 2012), while the latter result from gas to particle conversion processes, including NPF.

The occurrence of NPF in volcanic plume conditions was suspected in several earlier studies (e.g. Deshler et al., 1992; Robock, 2000; Mauldin et al., 2003), but the first dedicated study was conducted by Boulon et al. (2011), during the eruption of the

10   Eyjafjallajokull which happened in spring 2010. Indeed, using measurements performed at the high-altitude station of puy de Dôme (1465 m a.s.l., France), they linked the occurrence of NPF to unusually high levels of H_2SO_4 corresponding to model predictions of the Eyjafjallajokull plume transport to puy de Dôme, and highlighted a remarkably elevated particle formation rate in these conditions. While H_2SO_4 concentrations were derived from a proxy in this last study, Sahyoun et al. (in prep.) recently reported new evidence and quantification of the NPF process in the passive plumes of Etna and Stromboli, and

15   supported the key role of H_2SO_4 using direct measurement performed with a state-of-the-art mass spectrometer onboard the French research aircraft ATR-42. The rarity of studies dedicated to the observation of NPF in volcanic plume conditions is illustrated by the absence of any related topic in the recent review by Kerminen et al. (2018), despite the need for understanding such natural processes. Indeed, those might have dominated NPF and CCN formation in the pristine preindustrial era, when anthropogenic emissions were much lower. Our incomplete knowledge of the preindustrial conditions is responsible for a

20   significant fraction of the uncertainty on the impact of aerosols on climate, since these conditions form the baseline to calculate the radiative forcing caused by anthropogenic emissions in climate model simulations (Carslaw et al, 2013; Gordon et al, 2016, 2017). In specific, substantial uncertainties in the pre-industrial baseline cloud radiative state related to the activity of continuously degassing volcanoes were reported by Schmidt et al. (2012).

Despite providing new and highly valuable information, the studies by Boulon et al. (2011) and Sahyoun et al. (in prep.)

25   however had some limitations. Indeed, they were both based on short datasets, which did not allow for any statistical approach to evaluate the relevance of the process nor proper comparison with the occurrence of NPF outside of plume conditions. Also, airborne measurements conducted in the close vicinity of Etna and Stromboli allowed Sahyoun et al. (in prep.) to investigate the presence of the newly formed particles soon after the emission of their precursors from the vent of the volcanoes up to few tens of kilometres. They were however unfortunately not able to document properly the evolution of the particle size

30   distribution along the volcanic plumes, but analysed instead the particle concentration in relatively broad size ranges (2.5 – 10 nm, 10 – 250 nm). In addition, as mentioned earlier, this study was focussed on passive plumes, i.e. in the presence of a limited concurrent emission of primary particles by the volcanoes. Conducting similar investigation of active volcanic plumes is by the way more difficult due to the unexpected aspect of active eruptions. Taking the advantage of ground-based measurements and broader instrumental setup, Boulon et al. (2011) were in contrast able to study the time variation of the particle size

distribution between 2 nm and 20 µm, and, in turn, to evaluate the strength of the reported NPF events in terms of particle formation and growth rates. Measurements were however conducted after the active volcanic plume of Eyjafjallajokull had travelled several thousands of kilometres, and most likely underwent significant modifications due to the occurrence of chemical processes and dilution during transport.

5   In this context, the objectives of the present work were to provide new observations of NPF in an active volcanic plume with detailed analysis of the event characteristics, including the capacity of the newly formed particles to reach CCN sizes, and to assess the relevance of the process with respect to non-plume conditions. For that purpose, we used measurements of the particle number size distribution and SO_2 mixing ratios conducted at the Maïdo observatory (2165 m a.s.l., La Réunion island, Baray et al., 2013) between January 1st and December 31st 2015. During this period, 3 eruptions of the Piton de la Fournaise,

10   which is located in the south-eastern sector of the island (see Fig. 1.a from Tulet et al., 2017), were observed and documented, resulting in 36 days of measurement in plume conditions that could be compared with 250 "non-plume days". This dataset is, to our knowledge, the largest ever reported for the investigation of NPF in volcanic plume conditions.

2. Measurements and methods

2.1 Measurements

15   Measurements were performed at the Maïdo observatory located on La Réunion Island, in the Indian Ocean (21.080° S, 55.383° E) between January 1st and December 31st 2015. This high-altitude station (2165 m a.s.l.) is surrounded by lush tropical vegetation on the east side (natural amphitheatre of Mafate) and highland tamarin forest on the west side, which dominates the coast where the nearest urban areas of Saint Paul and Le Port are located (105 000 and 40 000 inhabitants, 13 and 15 km away from the station, respectively). The observatory was built in 2012, and since then it has been progressively equipped with a

20   growing instrumental setup dedicated to the monitoring of the upper troposphere and the lower stratosphere, including both in-situ and remote sensing techniques. Measurements conducted at Maïdo are of great interest since the observatory is one of the very few multi-instrumented stations in the tropics, and more particularly in the Southern hemisphere. Evidence of this is the involvement of the station in several international networks such as NDACC (Network for the Detection of Atmospheric Composition Change) and ACTRIS (Aerosol Cloud and Trace gases Research Infrastructure), and in the GAW (Global

25   Atmospheric Watch) regional network, which all ensure the quality of the data collected at this site. In addition, the proximity of the Piton de la Fournaise, located in the south-eastern region of the island ~ 39 km away from Maïdo, gives a strategic position to the station for the particular investigation of volcanic plume conditions, which are in the scope of the present work. More detailed information about the facility can be found in Baray et al. (2013) and Foucart et al. (2018), including a description of the large and local scale atmospheric dynamics which affect the observations performed at the site. An overview

30   of the monitoring of the volcanic plume performed at Maïdo during the eruptions of the Piton de la Fournaise observed in 2015 is in addition available in Tulet et al. (2017).

The instrumental setup used in the present work was previously described in the companion study by Foucart et al. (2018). The aerosol size distribution between 10 and 600 nm was measured with a custom-built Differential Mobility Particle Sizer (DMPS), with a time resolution of 5 min. Particles are first charged to equilibrium using a Ni-63 bipolar charger, after which they enter the DMPS, which includes a TSI-type Differential Mobility Analyzer (DMA) operating in a closed loop and a

5   Condensation Particle Counter model TSI 3010. The instrument was operated behind a Whole Air Inlet (higher size cut-off of 25 µm for an average wind speed of 4 m s^{-1}), and measurement protocols were defined with respect to the ACTRIS recommendations regarding both the flow rates and RH (Wiedensohler et al., 2012). The particle size distributions measured with the DMPS were used to detect the occurrence of NPF and to calculate the event characteristics, such as the particle formation and growth rates (see Sect. 2.2), and to further evaluate the potential of the newly formed particles to reach CCN

10   relevant sizes. DMPS data was also used to calculate the condensation sink (CS), which describes the loss rate of gaseous precursors on pre-existing particles (Kulmala et al., 2012). In addition to DMPS, an Air Ion Spectrometer (Airel, Estonia, Mirme et al., 2007) was operated at Maïdo between May and October 2015. The AIS includes two DMA which allow simultaneous detection of negative and positive ions and charged particles in the mobility range 0.0013-3.2 cm^2 V^{-1} s^{-1}, corresponding to mobility diameter 0.8-42 nm in NTP-conditions (Mäkelä et al., 1996). Each analyser is working with a flow

15   rate of 90 L min^{-1} (sample flow rate of 30 L min^{-1} and sheath flow rate of 60 L min^{-1}) in order to reduce diffusion losses in the instrument, and measurements were conducted through an individual short inlet (30 cm) to further limit the loss of ions in the sampling line. AIS data was collected with a time resolution of 5 min and was analysed in the present work to get further insight into the timing of the early stages of the NPF process.

SO$_2$ mixing ratios used to monitor the occurrence of volcanic plume conditions at Maïdo were measured with a UV

20   fluorescence analyser (Thermo Environmental Instrument TEI 43) operated by ATMO-Réunion (formerly referred to as ORA, Observatoire Réunionnais de l'Air), with a time resolution of 15 min. The detection limit of the instrument was about 0.5 ppb, which is above the usual SO$_2$ mixing ratios encountered at Maïdo outside of the eruptive periods of the Piton de la Fournaise (see Fig. A1 in Foucart et al. 2018).

Finally, meteorological parameters recorded with a time resolution of 3 s were used as ancillary data. Global radiation was

25   measured with a Sunshine Pyranometer (SPN1, Delta-T Dvices Ltd., resolution 0.6 W m^{-2}), and other variables of interest including temperature, wind speed and direction and relative humidity (RH) were recorded using a Vaisala Weather Transmitter WXT510.

An overview of the data availability for all abovementioned instruments between January 1st and December 31st 2015 is provided in Foucart et al. (2018, Fig. 2).

30   ## 2.2 Particle formation and growth rates

As previously reported in Foucart et al. (2018), the formation rate of 12 nm particles (J_{12}) expressed in cm^{-3} s^{-1} was calculated based on DMPS data following Kulmala et al. (2012):

$$J_{12} = \frac{dN_{12-19}}{dt} + CoagS_{12} \times N_{12-19} + \frac{GR_{12-19}}{7\,nm} \times N_{12-19} \qquad (1)$$

where N_{12-19} (cm^{-3}) is the number concentration of particles in the diameter range 12-19 nm, $CoagS_{12}$ (s^{-1}) represents the coagulation sink of 12 nm particles on larger particles and GR_{12-19} (nm h^{-1}) is the particle growth rate between 12 and 19 nm. The second and third terms on the right-hand side of Eq. (1) thus represent the loss rate of particles in the range 12-19 nm due to coagulation on pre-existing larger particles and condensational growth outside of the size range, respectively. Together with the production term J_{12}, these loss terms determine the time evolution of the particle concentration in the range 12-19 nm, denoted as $\frac{dN_{12-19}}{dt}$. GR_{12-19} was estimated from DMPS data based on the "Maximum method" introduced by Hirsikko et al. (2005). Briefly, the times t_m when the maximum concentration successively reached each of the DMPS size bins between 12 and 19 nm were first determined by fitting a normal distribution to the concentration time series of each bin. GR_{12-19} was then obtained by fitting a linear least square fit through the t_m values previously identified.

In order to get further insight into the early stages of the NPF process, and in absence of direct measurement of sub-3 nm particles, J_{12} and GR_{12-19} were used to derive the formation rate of 2 nm particles (J_2) following the equation from Lehtinen et al. (2007):

$$J_2 = \frac{J_{12}}{exp\left(-\gamma \times 2\,nm \times \frac{CoagS_2}{GR_{12-19}}\right)} \qquad (2)$$

where,

$$\gamma = \frac{1}{m+1}\left[\left(\frac{12\,nm}{2\,nm}\right)^{m+1} - 1\right] \qquad (3)$$

and,

$$m = \frac{log(CoagS_{12}) - log(CoagS_2)}{log(12\,nm) - log(2\,nm)} \qquad (4)$$

In Eq. (2) and (4), $CoagS_2$ represents the coagulation sink of 2 nm particles on larger particles.

2.3 Detection of the volcanic plume

Four eruptions of the Piton de la Fournaise were observed in 2015: the first in February, the second in May, the third at the very beginning of August, and, the last, from the end of August to late October. More details about the exact dates and characteristics of the eruptions can be found in Tulet et al. (2017). The Maïdo was considered to be in volcanic plume conditions when at least one of the hourly averages of the SO$_2$ mixing ratio measured between 06:00 and 11:00 LT (UTC +4) was ≥1 ppb, which corresponds to the 97th percentile of SO$_2$ mixing ratio on non-eruptive days. The relatively low SO$_2$ mixing ratios observed outside of the eruptive periods reflect the low pollution levels characteristic of this insular station, located at high altitude in a region rarely subject to significant influence of pollution from continental origin. The specific time period

between 06:00 and 11:00 LT was chosen because it includes the usual nucleation hours at the site (see Sect. 3.1.2 and Foucart et al., 2018), as the main purpose of the present work is to evaluate the effect of volcanic plume conditions on NPF. This last criterion slightly differs from that introduced earlier by Foucart et al. (2018), who did not restrict the plume detection to morning hours, but focussed instead on daytime values, i.e. when global radiation > 50 W m^{-2}. Also, in order to avoid any

5   misclassification of the days, all data between 4th and 17th of February were excluded from the analysis, since the lack of SO$_2$ measurement prevented from a proper identification of the plume conditions at Maïdo during this eruptive period. Consequently, only the last three eruptions of the year 2015, which occurred in May and over the period August-October, are discussed in the present work.

In total, 38 days were classified as "plume days" following the abovementioned criteria, among which 2 were excluded from

10   further analysis due to DMPS malfunctioning. All these 36 days were previously classified as plume days by Foucart et al. (2018), who identified 45 plume days in total. The difference in the classifications arises from the different time windows investigated in the two studies, i.e. morning nucleation hours (this study) vs daytime (Foucart et al., 2018). In fact, plume conditions were detected after 11:00 LT on the 8 additional plume days reported by Foucart et al. (2018). The majority of the 36 plume days (29/36) were identified during the longest of the eruptions of the Piton de la Fournaise observed in 2015, which

15   occurred between end of August and late October. Six of the remaining plume days were detected in May, and the last day was identified during the very short eruption observed in late July – early August.

In addition to the abovementioned classification, we further analysed the characteristics of the plume days in terms of 1) the duration of the plume conditions detected at Maïdo (from 1 to 5 hours between 06:00 and 11:00 LT) and 2) the level of the hourly average SO$_2$ mixing ratios measured during the same time period. The plume was detected during the 5 hours of the

20   time window of interest on 20 of the 36 days, and during 4 and 3 hours on 5 and 4 days, respectively. More sporadic appearance of plume conditions during 1 or 2 hours were only observed on 7 days, indicating that 80% of the plume days were characterized by plume conditions lasting during at least 3 hours between 06:00 and 11:00 LT. Concerning the SO$_2$ levels, they varied significantly from day to day. As an indicator of the "strength" of the plume, we calculated for each plume day the median of the SO$_2$ hourly averages ≥1 ppb identified between 06:00 and 11:00 LT. For 12 of the 36 plume days, the median

25   SO$_2$ level was found between 1 and 2 ppb, and 18 days showed median level relatively homogeneously distributed in the range between 2 and 14 ppb. Higher median SO$_2$ mixing ratios were observed on the remaining days, up to 249 ppb on the 20th of May. Based on this analysis, and in order to evaluate more specifically the effect of "strong" plume conditions on NPF (regarding both the duration of the plume conditions and the magnitude of the SO$_2$ levels), we further defined a sub-class of plume days, hereafter referred to as "strong plume days". The strong plume days were defined as plume days for which 1) the

30   plume conditions lasted from 06:00 to 11:00 LT, with 2) the median of the SO$_2$ hourly averages ≥ 5 ppb. In total, 14 days were classified as strong plume days based on these criteria. Note that these days were included in the statistics reported for plume days in the next sections, and were in addition highlighted separately. The threshold of 5 ppb was chosen as it led to a fair compromise between the number of days to be classified as strong plume days, which we wanted to keep significant for the

relevance of our analysis, and a mixing ratio of SO_2 significantly higher than that measured during non-eruptive periods. For comparison, 5 ppb corresponds to intermediate mixing ratios reported for polluted megacities (Mallik et al., 2014).

2.4 Sulfuric acid concentration in the gas phase

In the absence of direct measurements, we used a proxy to estimate the concentration of gaseous sulfuric acid. To our knowledge, there is no specific proxy dedicated to the rather unusual volcanic plume conditions, so we considered instead the expressions from Petäjä et al. (2009) and Mikkonen et al. (2011), which have already been widely used in nucleation studies. The two proxies have the common feature to consider the oxidation of SO_2 by OH as the only source of H_2SO_4, and do not include the contribution of other oxidants possibly emitted together with SO_2 in the volcanic plume, and possibly prone to contribute to H_2SO_4 production, as discussed earlier by Berresheim et al. (2014) for the coastal atmosphere. The two proxies however differ in their construction, as Petäjä et al. (2009) used data collected solely in the boreal forest, while Mikkonen et al. (2011) used measurements from different locations, including the urban area of Atlanta, where, to a certain extent, SO_2 mixing ratios are resembling those measured at Maïdo in plume conditions. Besides the variety of measurement conditions, the expression from Mikkonen et al. (2011) also considers more parameters, including the temperature dependant reaction rate between SO_2 and OH as well as the relative humidity, which can fluctuate a lot and reach high values at mountain sites such as Maïdo. Given the above, the proxy developed by Mikkonen et al. (2011) was finally used in the present work.

3. Results

3.1 NPF analysis in the volcanic plume

3.1.1 Frequency of occurrence

As mentioned in Section 2.3, 36 plume days were identified at Maïdo as a consequence of the 3 eruptions of the Piton de la Fournaise which could be documented in 2015. Besides the plume days, 250 days with no influence of the volcanic plume were identified and included in the analysis (days with plume conditions detected in the afternoon were excluded, 8 days in total, see Sect. 2.3 for more details); these days will be hereafter referred to as "non-plume days". Figure 1 shows the monthly NPF frequency separately for plume and non-plume days, with a specific focus on May, August, September and October 2015, when the eruptions were observed. Note that statistics for non-plume days were previously reported for all months in 2015 by Foucart et al. (2018). Our results suggest that volcanic plume conditions favour the occurrence of NPF at Maïdo since all the plume days were classified as NPF event days with the exception of 5 days classified as undefined in September, leading to higher NPF frequencies in plume conditions compared to non-plume days over the months highlighted on Fig. 1 (86% vs 71%). Focussing on the strong plume days, 12 were classified as event days and the remaining two days were classified as undefined. At the annual scale, i.e. when including all months in the calculation, the NPF frequency was raised from the already remarkably high value of 66.8% when excluding the plume days to 69.2% when considering both plume and non-plume days.

Such values are among the highest in the literature, similar to those previously reported for the high-altitude station of Chacaltaya (5240 m a.s.l., Bolivia) (64%, Rose et al., 2015) and the South African savannah (69%, Vakkari et al., 2011), slightly lower compared to that reported for the South African plateau, where NPF events are observed on 86% of the days (Hirsikko et al., 2012).

5 In addition, a quick analysis was also performed on the 8 days for which the volcanic plume was detected after the morning hours during which nucleation is usually initiated (see Section 3.1.2 for more details about the timing of NPF). With the exception of one day classified as undefined in October, all other days were classified as NPF event days, but there was no clear evidence of an effect of the "late" plume conditions on the ongoing events, triggered earlier during the day. High SO_2 mixing ratios (up to 78 ppb) associated to plume conditions were also measured during the night, but they were not

10 accompanied by any obvious particle formation nor growth process at Maïdo, supporting a determinant role of photochemistry in these secondary particle formation processes.

3.1.2 Timing of the events

As a first investigation of the specificities of NPF in plume conditions, we performed a simple analysis of the starting time of the NPF events on plume and non-plume days. The starting time of an event was defined by a visual inspection as the time

15 when the 1.5-2.5 nm ions concentration measured with the AIS significantly increased. Only the events simultaneously detected with the AIS and the DMPS were included in this analysis, and the dataset was not limited to May-August-September-October, but included instead all available AIS data between mid-May and end of October. In total, 37 events observed on non-plume days and 14 events detected in plume conditions were documented.

The median starting time of NPF in non-plume conditions was found at 08:32 LT [25th percentile: 08:14 LT; 75th percentile:

20 09:06 LT]. Earlier rising time of the cluster concentration was observed on plume days, around 07:48 LT [07:21 LT; 08:24 LT]. In addition, we also calculated the median time laps between sunrise and beginning of NPF, since the starting time of NPF was most likely affected by the change in sunrise time over the course of the investigated period. Median time laps between sunrise and rising time of the cluster concentration was 2h10 [1h49 ; 2h26] on non-plume days, with a minimum of 35 min observed on October 28th, and was about half an hour shorter in plume conditions, being 1h32 [1h03 ; 2h00], with a

25 minimum of 29 min obtained on August 28th. These observations suggest that on plume days, when precursors related to volcanic plume conditions were available prior to sunrise in a sufficient amount, photochemistry was the limiting factor for NPF to be triggered. In contrast, on non-plume days, NPF was certainly limited by the availability of condensable species, which were most likely transported from lower altitude by the mean of convective processes taking place after sunrise. Further discussion on the precursors involved in the process is reported in Sec. 3.2.2.

30 ### 3.1.3 Particle formation and growth rates

Figure 2 shows the formation rate of 2 and 12 nm particles (J_2 and J_{12}, respectively), as well as the particle growth rate between 12 and 19 nm (GR_{12-19}). Note that statistics reported for plume days do include data from the strong plume days, which are

in addition highlighted separately. Besides the high values observed on some of the strong plume days, which exceed those measured on regular plume days, GR_{12-19} showed an important variability, and with the exception of May, the monthly medians of GR_{12-19} were higher on non-plume days compared to plume days (Fig. 2.a). The overall effect of the plume conditions on the particle growth thus appeared to be limited. However, assessing the real effect of these specific conditions

5   on the particle growth is challenging. Indeed, as previously highlighted in the companion study by Foucart et al. (2018), the particle growth rates calculated from high altitude stations such as Maïdo are "apparent" due to the complex atmospheric dynamics around these sites, and may in particular be overestimated due to the concurrent transport of growing particles to the site.

In contrast, the effect of plume conditions was more pronounced on the particle formation rates, both for J_2 and J_{12} (Fig. 2.b

10   and c). Indeed, with the exception of September, when comparable median values were found on plume and non-plume days, the particle formation rates were on average increased on plume days, with the most important difference observed in May, when median J_2 and J_{12} were increased by a factor of ~17 and 7.5, respectively, in plume conditions. However, most of the values obtained on strong plume days were similar to those measured during regular plume days of the same month.

These observations suggest that, despite a limited effect on particle growth, plume conditions do affect NPF, both in terms of

15   frequency of occurrence and particle formation rate. Influence of the volcanic plume on larger particles, including CCN relevant sizes, is further investigated in Sect. 3.3., while the next section is focussed on the analysis of key atmospheric components previously reported to influence NPF.

3.2 Effect of key atmospheric components on the NPF process

3.2.1 Condensation sink

20   As recalled in Sect. 2.1, the condensation sink represents the loss rate of precursor vapours on pre-existing larger particles, and is thus expected to affect directly the amount of precursors available for NPF. In order to further investigate the effect of this parameter on the occurrence of NPF and avoid any interference with the CS increase caused by the newly formed particles themselves, we focus here on the CS observed prior to usual nucleation hours, between 05:00 and 07:00 LT.

Figure 3.a. shows the monthly median of the CS calculated over the abovementioned time period, separately for plume, strong

25   plume and non-plume days, event and non-event days. Note that strong plume days were included in the statistics reported for plume days, and were also highlighted separately. The comparison of non-plume NPF event and non-event days did not highlight any clear tendency over the months of interest for this study. Indeed, comparable median CS were observed in August regardless the occurrence of NPF later during the day, higher values were in contrast obtained on non-event days in May, while the opposite was observed in September and October, most likely related to biomass burning activity in South Africa and

30   Madagascar during austral spring (Clain et al., 2009; Duflot et al., 2010; Vigouroux et al., 2012). The overall number of non-event days included in the statistics was however limited, and using comparable time window Foucart et al. (2018) reported that CS was on average higher on NPF event days compared to non-event days when including all the data from 2015. These

contrasting results are representative of the observations from high altitude observatories at a larger scale, where both the location of the sites, their topography and the fast changing conditions related to complex atmospheric dynamics are likely to influence the effect of the CS on the occurrence of NPF. Indeed, Boulon et al. (2010) and Rose et al. (2015) reported that CS was on average positively correlated with the occurrence of NPF at Jungfraujoch (3580 m a.s.l., Switzerland) and Chacaltaya,

5   respectively. These observations suggest that the availability of the precursors was often limiting the process at these sites, which seemed to be fed with vapours transported together with pre-existing particles contributing to the CS. In contrast, the CS was observed to be on average lower on NPF event days compared to non-event days at puy de Dôme (1465 m a.s.l., France), which could be in a less precursor-limited environment due to its lower altitude.

Despite an important variability of the reported values, the median CS obtained on plume days were on average higher than

10   those observed on non-plume days, with the largest difference in May. The CS reported for strong plume days were even higher, with median values on average increased by one order of magnitude compared to non-plume event days (up to 30 times higher in May). One might have expected those enhanced CS to inhibit NPF at Maido, which was instead more frequent in plume conditions compared to non-plume days (Sect. 3.1.1). This non-intuitive result is most likely explained by the increased mixing ratios of SO_2 (Fig. 3.b), and in turn $[H_2SO_4]$ (see Fig. 4.b), which were concurrently measured on strong plume days.

15   Assuming that H_2SO_4 was contributing to NPF in such conditions, as previously suggested by Boulon et al. (2011) and Sahyoun et al. (in prep.), increased SO_2 emissions probably compensated for the strengthened loss rate of the vapours on plume days, and eventually let NPF occur. The involvement of H_2SO_4 in the NPF process is further investigated in the next section.

The origin of the particles responsible for increased CS prior to nucleation hours on plume event days remains uncertain, but the high SO_2 mixing ratios which were measured concurrently suggest a volcanic origin for these accumulation mode particles

20   (see Section 3.3.1 for more details about the shape of the particle number size distribution). The presence of accumulation mode particles emitted as primary ash have seldomly been reported in the literature, as the instrumentation used for volcanic studies are not adapted for measuring such small sizes. In the case of the Piton de la Fournaise, the existence of such particles was however very unlikely. Indeed, this basaltic volcano was reported to only emit negligible amount of ash, which were observed in the form of Pele's hairs during very specific eruptions (Di Muro et al., 2015); if present, we would have expected

25   the fragments of ash to also cause an increase of the particle mass in the coarse mode, which was not obvious during the eruptions observed in 2015 (Tulet et al., 2017). Other nocturnal sources of aerosols at the vent of the volcano and transport of these particles to Maïdo were in contrast more probable. A first possible production pathway is related to the fact that the Piton de la Fournaise is characterized by an usual water loading, reflected by high H_2O/SO_2 ratios (Tulet et al., 2017). In specific, there is continuous formation of liquid water at the vent of the volcano; gaseous SO_2 can thus be dissolved into the droplets,

30   leading to aqueous formation of H_2SO_4, which likely further condense onto pre-existing particles after evaporation of the cloud in the vicinity of the Piton de la Fournaise (Tulet et al., 2017). Catalytic oxidation of SO_2 inside the volcanic dome was also reported as a potential source of H_2SO_4 by Zelenski et al. (2015) based on measurements conducted at Bezymianny volcano. Finally, heterogenous formation of H_2SO_4 from H_2S occurring at the vent of the volcano, at high temperature, might also contribute to the observed particle loading. The abovementioned particles, originally formed or transformed *via* heterogeneous

mechanisms occurring in the very close vicinity of the vent, will be, despite the transformations they probably further undergo during their transport, referred to as volcanic primary particles hereafter, as opposed to secondary particles resulting from gas to particle conversion processes. These so-called primary particles are also likely to participate in daytime particle concentration, together with photochemically-driven secondary formation pathways.

3.2.2 The role of sulfuric acid

As previously mentioned in Sect. 2.4, sulfuric acid concentrations were obtained from SO_2 mixing ratios using the proxy by Mikkonen et al. (2011). H_2SO_4 has often been reported to play a key role in the early stage of atmospheric NPF (Sipilä et al., 2010; Kulmala et al., 2013; Yan et al. 2018), and in particular in sulfur-rich volcanic plume conditions (Mauldin et al., 2003; Boulon et al., 2011; Sahyoun et al., in prep.), thus motivating our specific interest in this study.

Figure 4.a shows all J_2 derived during the NPF events detected in plume conditions as a function of $[H_2SO_4]$. Highest $[H_2SO_4]$ were mostly observed on strong plume days and coincided with the highest J_2. In order to further investigate the relationship between the cluster particle formation rate and the abundance of H_2SO_4, J_2 was fitted with a simple power model $J_2 = k \times [H_2SO_4]^a$, in a similar way as previously done in earlier studies (Kulmala et al., 2006; Sihto et al., 2006; Kuang et al., 2008; Sahyoun et al., in prep.). When considering all data in the fitting procedure, i.e. including strong plume days, parameters k and a were found to be 6.75×10^{-10} and 1.07, respectively. When focussing on strong plume days only, slightly different fitting parameters were obtained, being 4.47×10^{-18} and 1.97 for k and a, respectively. In both cases the correlation between J_2 and $[H_2SO_4]$ was moderate, especially when limiting the analysis to strong plume days ($R^2 = 0.21$ and 0.11, for all plume days and strong plume days only, respectively), but still significant, as indicated by the corresponding p-values ($p = 5.77 \times 10^{-25}$ and 0.01, for all plume days and strong plume days only, respectively). As a reminder, the p-value is commonly used to quantify the statistical significance, and indicates in the context of this study the maximum probability for the correlation observed between J_2 and $[H_2SO_4]$ to result from a coincidence. Our results suggest that different mechanisms were likely to explain the observed formation rates across the investigated $[H_2SO_4]$ range, with stronger dependence on $[H_2SO_4]$ above 5×10^8 cm^{-3} observed on strong plume days, as one might have expected. Further investigation of this aspect and comparison with non-plume days was unfortunately not possible since SO_2 mixing ratios were mostly below the detection limit of the instrument outside of the eruptive periods of the Piton de la Fournaise.

The values calculated for k and a using all data (i.e. including strong and regular plume days) were slightly different from those reported by Kuang et al. (2008) for a set of 7 stations, including 2 insular marine sites in the Pacific Ocean and 5 urban or rural continental sites located in Northern America and Europe, where the authors systematically found a in the range 1.98-2.04 and k between $\sim 10^{-14}$ and 10^{-11}. These values were however calculated from a limited number of events for each site (from 1 to 9 events per site), and were derived from the correlation between J_1 (instead of J_2 in the present work) and measured $[H_2SO_4]$ (instead of proxy-derived in ours study). Also, none of the NPF events investigated by Kuang et al. (2008) occurred in volcanic plume conditions. Overall, the values derived on plume days at Maïdo were in contrast more consistent with those

Atmospheric Chemistry and Physics
10.5194/acp-2019-100
2019-02-08
journal article
en

recently reported by Sahyoun et al. (in prep.) based on aircraft measurements conducted in the passive plume of Etna ($k = 1.84 \times 10^{-8}$, $a = 1.12$), despite slight differences in the analysis. Indeed, Sahyoun et al. (in prep.) used direct measurements of [H_2SO_4] and investigated the link between [H_2SO_4] and $J_{2.5}$ instead of J_2. Also, instead of fitting all derived $J_{2.5}$, the dataset was first binned with respect to [H_2SO_4] (bins of equal length, 0.25×10^8 cm^{-3}), after which median $J_{2.5}$ were calculated for each

5   bin and finally fitted using a power model. As a sensitivity study, and in order to provide a more consistent comparison with the results reported by Sahyoun et al. (in prep.), we applied similar fitting method; only difference was in the binning procedure, as we used bins with an equal number of data points instead of equal length. The results of this analysis are shown on Fig. A1, in Appendix A. Applying the fit on median J_2 led to comparable fitting parameters ($k = 1.27 \times 10^{-9}$, $a = 1.00$), but the resulting correlation between J_2 and [H_2SO_4] appeared to be significantly stronger ($R^2 = 0.91$, $p = 1.57 \times 10^{-5}$). We also investigated the

10   impact of the number of bins on the final parameters and goodness of the fit (Table A1 in Appendix A), but varying the number of bins between 10 and 30 did not led to major differences.

In addition, we also compared J_2 derived from DMPS measurements with those predicted by the recent parameterization developed by Määttänen et al. (2018), which describes neutral and ion-induced H_2SO_4-H_2O particle formation. We used the Fortran code included in the supplementary electronic material of the paper, and, for each NPF event, we run the model using

15   measured values for temperature and relative humidity, CS values derived for DMPS measurements and [H_2SO_4] calculated with the proxy by Mikkonen et al. (2011). We used an average value of 3 cm^{-3} s^{-1} for the ion pair production rate, consistent with previously reported values from different sites, including the high-altitude station of puy de Dôme (Rose et al. 2013 and references therein). Otherwise, all settings and parameters were those set by default in the Fortran code. Figure 4.b shows, for the same dataset as in Fig. 4.a, the ratio between J_2 derived from DMPS measurements (referred to as J_{meas}) and J_2 predicted

20   by the parameterization (referred to as J_{param}), which included both neutral and ion-induced nucleation pathways. In addition, we also binned the data with respect to [H_2SO_4] (10 bins with equal number of points) and calculated the median ratio J_{meas}/J_{param} in each bin. As evidenced on Fig. 4.b, 60% of the calculated ratios were < 1, which was unexpected since particle formation rates resulting from the binary nucleation of H_2SO_4-H_2O should not exceed J_{meas}. This result was most likely related to 1) the use of proxy-derived [H_2SO_4] in the calculation of J_{param} and 2) the fact that J_{meas} was not derived from direct

25   measurement of 2 nm particles but from J_{12} and GR_{12-19}, which might have led to additional uncertainty. However, despite this inconsistency, Fig. 4.b illustrates our ability to predict J_2 from SO_2 mixing levels with a relatively fair accuracy, especially for [H_2SO_4] in the range between 1.5×10^8 and 6×10^8 cm^{-3}. Indeed, the medians of J_{meas}/J_{param} highlighted on Fig. 4.b indicates that J_{param} was on average within a factor of 5 of J_{meas} for [H_2SO_4] < 10^9 cm^{-3}. Higher discrepancies were in contrast observed for [H_2SO_4] > 10^9 cm^{-3}, which may stem from a reduced predictive ability of the proxy by Mikkonen et al. (2011)

30   for the highest SO_2 mixing ratios, since such values were not used in the construction of the proxy, or from the binary nucleation parameterization not being fully adapted to the volcanic plume environment. Nonetheless, despite the abovementioned limits, we believe that the last results are of high interest, because they show that in absence of direct measurement of [H_2SO_4] and sub-2nm particles concentration, the knowledge of SO_2 mixing ratios can lead to a fair approximation of J_2.

All together, these results suggest that higher SO$_2$ mixing ratios observed on plume days did contribute to the NPF events observed in such conditions, in agreement with earlier results from Boulon et al. (2011) and Sahyoun et al. (in prep.). However, the contribution of other compounds to the process could not be excluded based on the available dataset, and additional measurements would be needed to further investigate this aspect, including in specific direct measurement of the chemical composition of the clusters as well as their precursors.

3.3 Particle growth up to climate relevant sizes in the volcanic plume

The previous section was dedicated to the analysis of NPF occurrence and characteristics in volcanic plume conditions. In this section, we further investigate the effect of such process on the shape of the particle size distribution, first including all sizes between 10 and 600 nm, and then focussing more specifically on large-enough particles to act as CCN.

3.3.1 General features of aerosol particle size distributions

The effect of NPF and/or plume conditions on the particle number size distribution was investigated based on the hourly median particle spectra measured with the DMPS in different conditions between 07:00 and 16:00 LT (Fig. 5). This time period was selected as, besides usual NPF hours, it also includes one hour prior to nucleation hours, which allowed to study the main features of the particle size distribution in the different conditions (plume and non-plume) without fresh influence of NPF, as well as several hours to investigate the change of the spectra caused by particle growth processes. Note that in order to increase the statistical relevance of the results (especially for non-event days), the analysis was not restricted to May-August-September-October, and all available data was included in the analysis. All median spectra were in addition fitted with four Gaussian modes, including nucleation, Aitken and 2 accumulation modes, which parameters are shown on Fig. 6 and also reported in Table B1 of Appendix B. The spectra measured on strong plume days were included in the statistics reported for plume days and are also displayed separately on Fig. 5, but were however not independently fitted with Gaussian modes. Indeed, the uncertainty related to this procedure (and thus on the mode parameters themselves) was significantly increased because of 1) the limited number of days and 2) the important variability of the atmospheric conditions during these specific days.

As previously mentioned, the median spectra recorded at 07:00 LT, i.e. prior to nucleation hours, gave a unique opportunity to compare the main features of the particle number size distributions recorded in plume and non-plume conditions in absence of freshly nucleated particles. The spectra measured on non-plume days (both event and non-event days) displayed comparable shapes as well as similar concentrations, while higher concentrations were in contrast measured in plume conditions, and more specifically on strong plume days. As discussed in Section 3.2.1, these differences, which were the most pronounced for the 2 accumulation modes, were most likely explained by the presence of particles originating from heterogeneous processes occurring at high temperatures at the vent during the eruptive periods, and assimilated to volcanic primary particles Indeed, in plume conditions the population of the first accumulation mode (modal diameter ~100 nm) was on average around 235 cm^{-3}, against 55-80 cm^{-3} on non-plume days, indicating the presence of 155-180 cm^{-3} additional primary particles originating from

the volcano on plume days. Following similar reasoning, the contribution of volcanic primary particles to the concentration of the second accumulation mode (modal diameter ~190 nm) was around 68-82 cm^{-3}. Hence, there was more than a threefold increase in the accumulation modes particle number concentration due to the emission of primary volcanic particles. Regarding the diameters of the modes, they did not appear to be significantly affected by the different atmospheric conditions.

5   Despite some variations of the particle concentration in the different modes, the shape of the spectrum observed at 07:00 LT remained the same throughout the investigated time window on non-event days. The concentrations of the Aitken and first accumulation modes were increased by a factor of ~ 2 between 07:00 LT and 13:00 LT, from 130 to 310 cm^{-3} and 55 to 112 cm^{-3}, respectively, and concurrently the concentration of the second accumulation mode was multiplied by ~ 4, from 32 to 142 cm^{-3}, probably due to the transport of pre-existing particles from lower altitude. Surprisingly, the most important variation was

10   observed for the concentration of the nucleation mode, with a 5-fold increase from 18 to 80 cm^{-3} between 07:00 LT and 12:00 LT despite the absence of NPF. These concentrations were however significantly lower compared to those observed on NPF event days, up to 5800 cm^{-3} in plume conditions. Also, in contrast with NPF event days, the diameters of the modes, including in specific that of the nucleation mode, remained stable throughout the investigated time window (modal diameter ~15nm, ~36 nm, ~83 nm and ~164 nm for the nucleation, Aitken, first and second accumulation modes, respectively), indicating the absence

15   of a growth process characteristic of NPF.

Consistent with previous observations reported in Sect. 3.1.2, the starting of NPF was seen at 08:00 LT on event days (regardless the occurrence of plume conditions) from a visual analysis of the spectra, and was further confirmed by the increase of the particle concentration in the nucleation mode, which lasted until 11:00 LT. The most significant change was observed in plume conditions, with a thousand-fold increase of the nucleation mode particle concentration in 4 hours, from 5 to 5800

20   cm^{-3}, i.e. two orders of magnitude stronger than that observed on non-plume days (from 25 to 1700 cm^{-3}), consistent with the higher particle formation rates observed on plume days (see Sec. 3.1.2). After 11:00 LT, the particle concentration in the nucleation mode was observed to decrease, down to 290 cm^{-3} and 990 cm^{-3} at 16:00 LT, on plume and non-plume days, respectively, most likely because of the growth of particles outside of the mode, as well as their loss on larger particles through coagulation processes. Concurrent increase of the modal diameter was also observed between 07:00 and 13:00 LT on plume

25   days, from 12 to 25.5 nm, and slightly later, between 09:00 and 16:00 LT, on non-plume days, from 10 to 30 nm, further illustrating the simultaneous formation and growth of the particles.

Still focussing on NPF event days, the changes observed in the parameters of the Aitken and 2 accumulation modes were less pronounced than for the nucleation mode. With the exception of the slight difference observed at 07:00 LT, the Aitken mode displayed similar diameters on plume and non-plume days, with only limited variations over the investigated time window,

30   especially on non-plume days (31-45 nm and 38-46.5 nm, on plume and non-plume days, respectively). Also, the initial concentrations of the Aitken mode measured in the different conditions were similar, ~200 cm^{-3}, indicating that no primary particles of this size were produced by the volcano. The increase of the particle concentration observed until 13:00-14:00 LT was in contrast more pronounced on plume days (~ 10-fold increase in plume conditions, up to 2100 cm^{-3}, vs ~ 4-fold increase on non-plume days, up to 750 cm^{-3}), indicating the presence of ~1350 cm^{-3} additional particles in the Aitken mode due to the

presence of the plume. This observation was consistent with the enhanced production of particles previously reported for lower sizes in plume conditions, as the particles in the Aitken mode most likely resulted from the growth of smaller particles originating from the nucleation mode. As already mentioned, the concentrations of the 2 accumulation modes measured at 07:00 LT were both significantly higher on plume days (235 and 100 cm^{-3}, for the first and second accumulation mode, respectively) compared to non-plume days (80 and 18 cm^{-3}, respectively), most likely due to additional sources of particles at the vent of the volcano during eruptive periods (see Section 3.2.1). Later on, the transport of primary particles originating from the urban areas located at lower altitude as well as the growth of the newly formed particles most likely contributed to the concentration increase observed for the accumulation modes during the course of the nucleation period, up to 660 and 620 cm^{-3}, respectively, on plume days, against 445 and 130 cm^{-3} on non-plume days. With the hypothesis that vertical transport from the boundary layer was the same on plume and non-plume days, we could evaluate that the volcanic plume secondary aerosol formation contributed to ~ 220 cm^{-3} and ~ 490 cm^{-3} in the 1st and 2nd accumulation modes, respectively. Concerning the diameter of the modes, that of the second accumulation mode showed limited variations on plume days (188-203 nm), being closed to that observed on non-plume days (191 nm). In contrast, the initial diameter of the first accumulation mode was higher on non-plume days (97 vs 81.5 nm) and also showed a more pronounced increase up to 146 nm over the investigated time period.

Altogether, one can infer from these measurements a distribution of the particles of volcanic origin, including the contributions of both primary and secondary aerosols. Following the above analysis, the concentration of the so called volcanic primary particles was calculated for each mode as the difference between the concentrations measured at 07:00 LT on plume and non-plume days, and the values obtained at 07:00 LT in plume conditions were used for the other characteristics of the modes (i.e. sigma and modal diameter). In addition, the concentration of secondary aerosol particles of volcanic origin was calculated for each mode as the difference between the maximum concentration observed on plume event days and that observed on non-plume event days; the values obtained at 12:00 LT in plume conditions, when the effect of secondary aerosol formation on the spectrum was on average the most pronounced, were used for the other characteristics of the modes. Resulting aerosol spectrum is reported on Fig. 7, with the detailed contributions of volcanic primary and secondary particles for each mode. Secondary aerosol particles formed due to the presence of the plume contributed 96% of the total concentration observed on plume event days, clearly dominating all the modes but the first accumulation mode, for which the contribution of volcanic primary particles was more significant.

3.3.2 Investigation of the formation of potential CCN during NPF events

The increase of potential CCN concentration during NPF was investigated using DMPS measurements, in a similar way as done earlier by Rose et al. (2017) for the high-altitude station of Chacaltaya, following the approach originally developed by Lihavainen et al. (2003). It is based on the hypothesis that the lower cloud droplet activation diameter d_{act} of aerosol particles is in the range 50 – 150 nm for the typical supersaturations (SS) encountered in natural clouds, including those forming at high altitude (Jurányi et al., 2011; Hammer et al., 2014). For instance, direct CCN measurements conducted at the high altitude

station of puy de Dôme with a dedicated chamber (Roberts and Nenes, 2005) showed that particles in the range 50-150 nm were activated at SS 0.24%, also reported to be representative of in-cloud SS at the site (Asmi et al., 2012). Following this basic assumption, the concentration of potential CCN can be assimilated to the particle concentration $N_{>d_{act}}$ measured above any given d_{act} in the range 50 - 150 nm. Sensitivity studies are usually performed using multiple activation diameters, which

5 reflect the effect of both the properties of the particle itself (such as the chemical composition) and atmospheric conditions (such as the supersaturation) on the ability of a particle to activate into a cloud droplet (e.g. Kerminen et al. 2012 and references therein). We used in a first approach the same activation diameters (50, 80 and 100 nm) as Rose et al. (2017), and we based our analysis on both the time series of the concentration of particles larger than these thresholds (hereafter referred to as N_{50}, N_{80} and N_{100}, for 50, 80 and 100 nm, respectively) and the overall shape of the event reflected by the corresponding surface

10 plot. This indirect method based on DMPS measurements only provides estimations of potential CCN concentrations instead of real concentrations as measured by CCN chambers (Roberts and Nenes, 2005); however, for simplicity, we refer to these potential CCN as CCN hereafter.

This last analysis was not restricted to the months when the volcanic activity was detected, and all 198 NPF event days identified in 2015 were included in the analysis (167 non-plume days and 31 plume days). As reported earlier by Foucart et al.

15 (2018), the growth of particles > 80 – 100 nm was observed as a common feature of a large majority of the investigated days besides NPF, regardless the occurrence of plume conditions. In addition, high background concentrations were frequently seen above ~ 50 nm, most likely caused by the transport of pre-existing particles to the station. The influence of these phenomena on the variations of N_{80} and N_{100} was obvious, and often hindered the identification of a concurrent impact of NPF on the particle concentration increase at these sizes. In contrast, the background concentration was often significantly lower at 50 nm,

20 which made it easier to unambiguously assess the growth of the newly formed particles up to 50 nm. Further evaluation of the contribution of NPF to the formation of CCN was thus finally performed using this single activation diameter, assuming N_{50} was a good proxy for the concentration of particles likely to act CCN, or to become CCN after experiencing further growth.

The increase of N_{50} observed during the events was attributed (at least partly) to NPF on 75 days, 20 of them being plume days, among which 8 strong plume days, and the remaining 55 being non-plume days. On the other 123 event days included

25 in the analysis, the contribution of NPF to the increase of N_{50} was more uncertain, but could not be excluded. Resulting frequencies of NPF contributing to the increase of > 50 nm CCN were thus 33.2% for non-plume days, 64.5% for plume days (including strong plume days) and 66.7% for strong plume days alone (Fig. 8.a). The increase of N_{50} observed during NPF was in addition quantified: N_{50-MAX}, the maximum of N_{50} observed during the event was compared to N_{50-REF}, calculated as the two-hour average of N_{50} between 05:00 and 07:00 LT, prior to nucleation hours. Note that for a given NPF event, the

30 identification of N_{50-MAX} was limited to the time period 07:00 - 19:00 LT, because of the fast change of air masses and / or wind direction which is often observed at Maïdo after 19:00 LT (see Fig. C1 in Appendix C). The absolute increase of N_{50} was further calculated as the difference between N_{50-MAX} and N_{50-REF}, and the median CCN productions observed in the different conditions are reported on Fig. 8.b. The median of the N_{50} absolute increase observed on non-event days was around

420 cm^{-3}, and was significantly enhanced on event days, being around 1600 cm^{-3} on non-plume days and 2530 cm^{-3} in plume conditions, reaching up to 3170 cm^{-3} when focussing on strong plume days only. The more pronounced concentration increase observed on event days, and in specific in plume conditions, was explained by the multiplication of the sources of such particles on those specific days. Indeed, on non-event days, the variations of N_{50} observed at Maïdo were probably caused exclusively

5 by the transport of pre-existing large particles originating from the nearest urban areas. This process was itself tightly connected to the dynamics of the boundary layer and associated wind pattern, resulting in maximum concentrations around 13:00 LT (i.e. 09:00 UTC), as evidenced on Fig. 8.d. On event days, the diurnal variation of N_{50} was strengthened due to the concurrent formation of secondary aerosols, i.e. including the formation and growth of new particles as well as the growth of pre-existing larger particles mentioned earlier (Fig. 8.d). Additional contribution of large particles formed *via* heterogeneous processes

10 close to the vent of the volcano (and denoted as volcanic) primary particles in the present work was finally highly probable in plume conditions, as discussed in Sections 3.2.1 and 3.3.1. This last hypothesis was further supported by the increased level of N_{50} observed during the night on plume days, and especially on strong plume days, compared to other days (Fig. 8.d).

In a similar way as done previously by Rose et al. (2017), we made an attempt to decouple the contributions of the abovementioned CCN sources on event days. For that purpose, the transport of pre-existing large particles from the boundary

15 layer was first assumed to have similar magnitude on event and non-event days, regardless the occurrence of plume conditions. We also made the assumption that the contribution of volcanic primary particles did not vary significantly along the day in plume conditions, and was thus systematically removed when calculating the difference between N_{50-MAX} and N_{50-REF}. Following these hypotheses, the contribution of secondary aerosols to the observed CCN population was estimated from the difference between the median of the N_{50} absolute increase observed on event days (i.e. resulting from transport of particles

20 from the boundary layer and secondary aerosol formation) and that of non-event days (resulting from transport only). Resulting concentrations attributed to secondary aerosols were ~ 1180 cm^{-3}, ~ 2110 cm^{-3} and ~ 2750 cm^{-3} for non-plume, plume and strong plume event days, respectively, and dominated the increase of N_{50} observed on event days. From these average concentrations we could also infer the formation of secondary aerosols prone to act as CCN in plume conditions, with ~ 930 cm^{-3} additional particles detected on regular plume days and ~ 1570 cm^{-3} on strong plume days compared to non-plume days.

25 This stronger increase of the CCN concentration was most likely explained by the larger amount of condensable vapours available in plume conditions, including in specific sulfuric acid, as evidenced on Fig. 8.c. Indeed, the most significant N_{50} increases coincided with high [H$_2$SO$_4$], suggesting that the growth of the newly formed particles to CCN relevant sizes was favoured during NPF events occurring in the presence of large amount of H$_2$SO$_4$ caused by the eruptions. The increase of N_{50} due to secondary aerosol formation in the presence of the plume was also consistent and of the same order of magnitude as the

30 increase of the particle concentration reported in similar conditions for the Aitken and accumulation modes in the previous section.

4. Conclusion

We investigated the occurrence of NPF in volcanic plume conditions at the Maïdo observatory based on measurements conducted between January 1st and December 31st 2015. During this time period, 4 effusive eruptions of the Piton de la Fournaise, located ~39 km away from the station, were observed, and we were able to detect volcanic plume conditions at

5   Maïdo during 3 of the 4 eruptions. In total, 36 "plume days" were identified according to SO_2 mixing ratios measured during morning hours (06:00 – 11:00 LT, i.e. including usual nucleation hours), among which 14 days classified as "strong plume days", and were compared with 250 "non-plume days". This dataset is, to our knowledge, the largest ever reported for the investigation of NPF in volcanic plume conditions, and allowed for the first time a statistical approach to characterize the process and also assess its relevance with respect to non-plume conditions.

10 Focussing on the months during which the volcanic plume was detected at Maïdo (May, August, September and October), NPF was observed on 86% of the plume days vs 71% of the non-plume days. On plume days, when higher amounts of precursors (such as SO_2) were available prior to sunrise due to the occurrence of plume conditions, NPF seemed to be mainly limited by photochemistry, and was triggered early after sunrise. The process was in contrast observed later on non-plume days, most likely due to the lack of precursors before their transport from lower altitudes after sunrise, as a result of convection.

15 Despite high values of GR_{12-19} reported on strong plume days, the overall effect of plume conditions on particle growth between 12 and 19 nm appeared to be limited. In contrast, with the exception of September, particle formation rates, both J_{12} and J_2, were on average significantly increased on plume days.

Signature of the volcanic plume on the aerosol spectra up to 600 nm was further investigated based on the analysis and fitting of the particle size distributions recorded in the different conditions. The spectra measured prior to nucleation hours (07:00

20 LT) gave a unique opportunity to compare the main features of the particle number size distributions recorded in plume and non-plume conditions in absence of freshly nucleated particles. Main differences were observed for the two accumulation modes (modal diameter ~ 100 and 190 nm, respectively), which were more densely populated in plume conditions compared to non-plume days, most likely because of the contribution of particles formed *via* heterogeneous processes at the vent of the volcano during eruptive periods, and assimilated to primary volcanic particles in the present work. The particle size distribution

25 only experienced limited changes on non-event days, but significant variations of the particle concentration were in contrast observed for the nucleation and Aitken modes on NPF event days between 08:00 and ~11:00 LT, especially in plume conditions. An average size distribution of the particles of volcanic origin was further inferred from the measurements performed on event days in and off-plume conditions. The contribution of secondary particles to the total concentration was around 96%, and clearly dominated that of primary particles for all but the first accumulation mode concentration, for which

30 primary particles contributed significantly (52%).

Specific attention was further paid to the concentration of particles > 50 nm (N_{50}), assuming they could be used as a proxy for potential CCN population. The variations of N_{50} were limited on non-event days, and attributed mainly to the vertical transport of pre-existing particles from the boundary layer, evaluated to ~ 420 cm^{-3}. The contribution of secondary particles to the

increase of N_{50} was more frequent in plume than off-plume conditions, and the magnitude of the increase due to secondary aerosol formation was ~ 2110 cm^{-3} compared to ~1180 cm^{-3} on non-plume days.

In order to investigate deeper the influence of volcanic plume conditions on the occurrence of NPF and related effects on particle concentration, attention was paid to the variations of the condensation sink (CS) and [H$_2$SO$_4$], previously reported to

5   play a key role in the process. In order to avoid any interference with the CS increase caused by the newly formed particles themselves, we focussed on the CS slightly prior to nucleation hours. The comparison of non-plume NPF event and non-event days did not highlight any clear tendency over the months of interest for this study. In contrast, the median CS obtained on plume days were on average higher than those observed on non-plume days. Increased SO$_2$ mixing ratios measured concurrently in plume conditions most likely compensated for the strengthened loss rate of the vapours and let NPF happen,

10 suggesting at the same time a key role of H$_2$SO$_4$ in the process, consistent with recent observations in the plumes of Etna and Stromboli (Sahyoun et al., in prep.). In order to test this last hypothesis, we derived [H$_2$SO$_4$] from SO$_2$ mixing ratios using a proxy available in the literature (Mikkonen et al., 2011). Despite a moderate strength, the correlation between J_2 and [H$_2$SO$_4$] was found to be significant. In addition, we also evaluated the contribution of binary nucleation of H$_2$SO$_4$ – H$_2$O to the observed events using the recent parameterization by Määttänen et al. (2018). Within the uncertainties associated to our calculations,

15 we showed that in plume conditions, predicted J_2 from calculated H$_2$SO$_4$ concentration were fair approximations of J_2 derived from the measured J_{12}, indicating that H$_2$SO$_4$ was the main nucleating species in the plume. This result also highlighted the possibility to get relatively good estimates of J_2 in absence of direct measurement of [H$_2$SO$_4$] and sub-2nm particles concentration, but only from the knowledge of SO$_2$ mixing ratios.

All together, our observations show that, based on one year of data, volcanic plume conditions favour the formation of particles

20 that frequently grow to CCN sizes within the first 40 km of the volcano's vent. The quantification of the contribution of primary vs secondary aerosol formation within an active volcanic plume on a statistical basis contributes to better understanding of this natural process, which might have contributed significantly to NPF and CCN formation in the pristine preindustrial era. Nonetheless, our study should be complemented in the future with a direct analysis of the precursor vapours involved in the process, as our approach to assess the role of H$_2$SO$_4$ was based on calculations and we cannot exclude the contribution of other

25 compounds, such as for instance halogens, and in particular iodine compounds, which were previously identified in volcanic plumes (Aiuppa et al., 2009) and also reported to contribute to NPF in coastal zones (Sipilä et al., 2016).

5. Data availability

SMPS data are accessible from the EBAS website (http://ebas.nilu.no/). AIS and SO$_2$ data can be provided upon request.
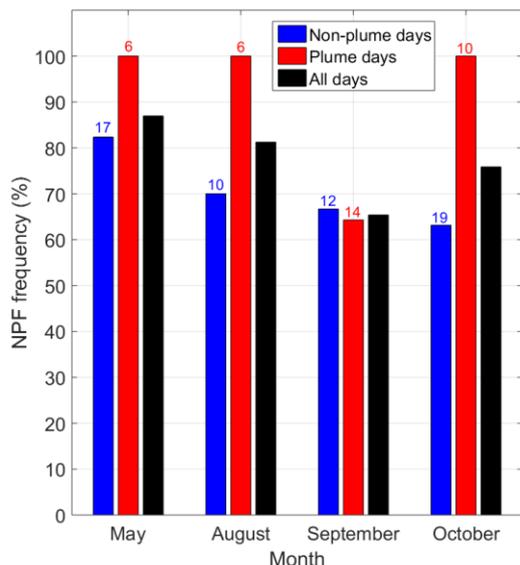
Figure 1 Frequency of occurrence of NPF at Maïdo. Statistics are shown separately for plume and non-plume days, and total frequencies are also reported. Numbers on the plot indicate, for plume and non-plume conditions, the total number of days included in the statistics.
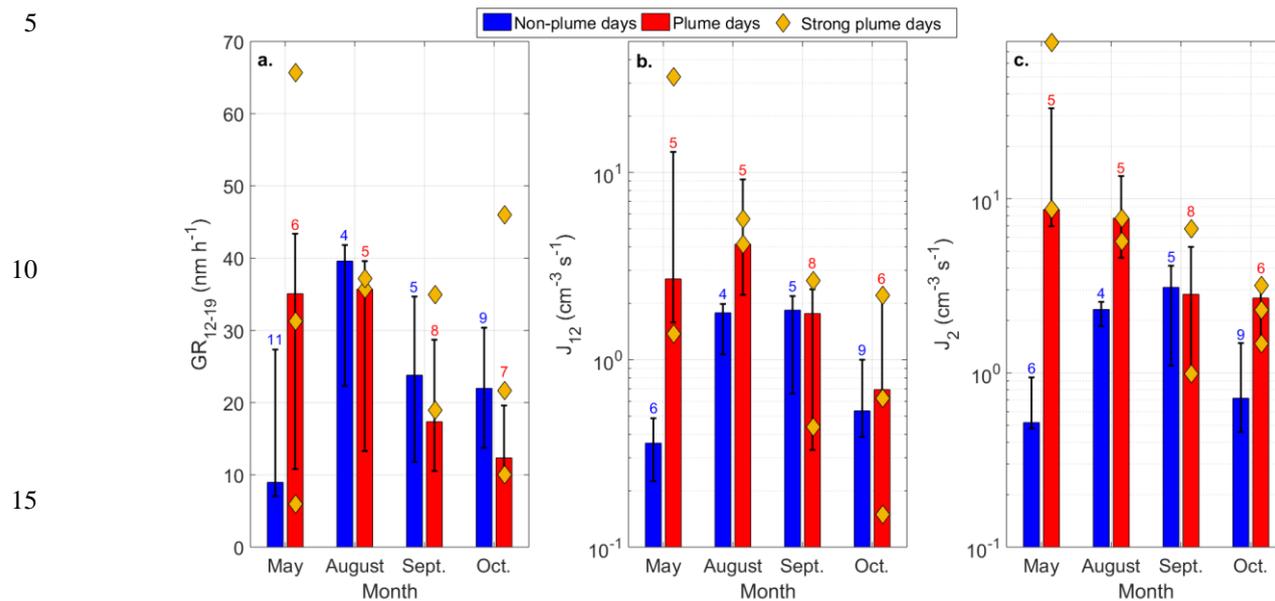
Figure 2 Monthly medians and percentiles of the NPF event characteristics observed on plume and non-plume days at Maïdo. a. Particle growth rate between 12 and 19 nm (GR_{12-19}). Formation rate of b. 12 (J_{12}) and c. 2 nm (J_2) particles. The bars represent the median of the data, and the lower and upper edges of the error bars indicate 25th and 75th percentiles, respectively. Data collected on strong plume days are
20 included in the statistics reported for plume days and are also highlighted separately. Numbers on each plot indicate, for plume and non-plume conditions, the total number of NPF events included in the statistics.
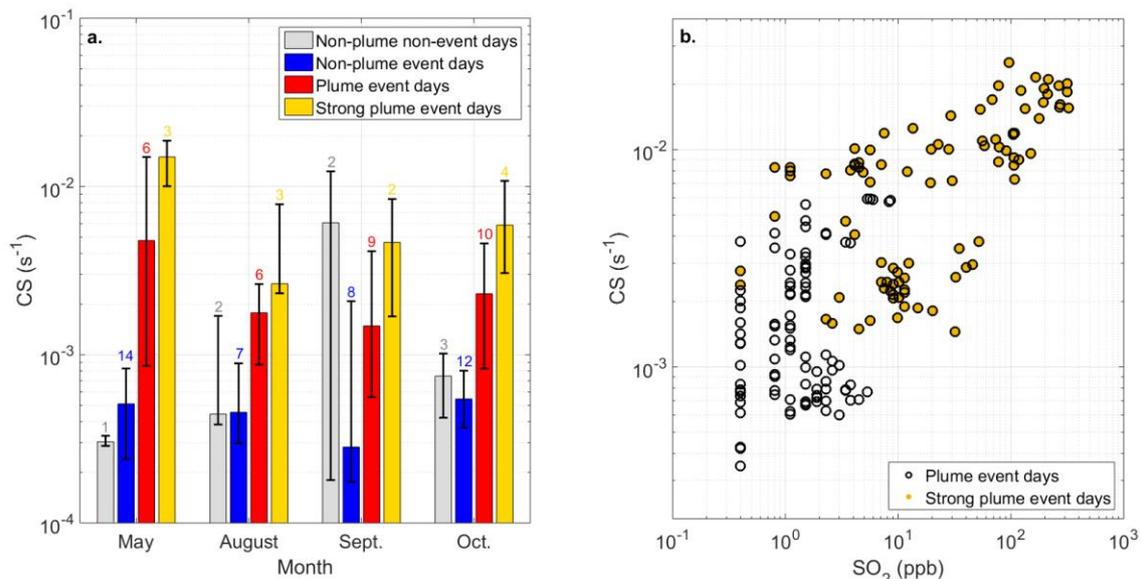
Figure 3 a. Monthly medians and percentiles of the CS measured prior to NPF hours (i.e. 05:00-07:00 LT). Note that strong plume days are included in the statistics reported for plume days and are also highlighted separately. See Fig. 2 for an explanation of symbols. Numbers on the plot indicate, for plume and non-plume conditions, event and non-event days, the total number of days included in the statistics. b. Link between the CS measured prior to NPF hours and SO_2 mixing ratios on plume days. Strong plume days are highlighted with specific markers.
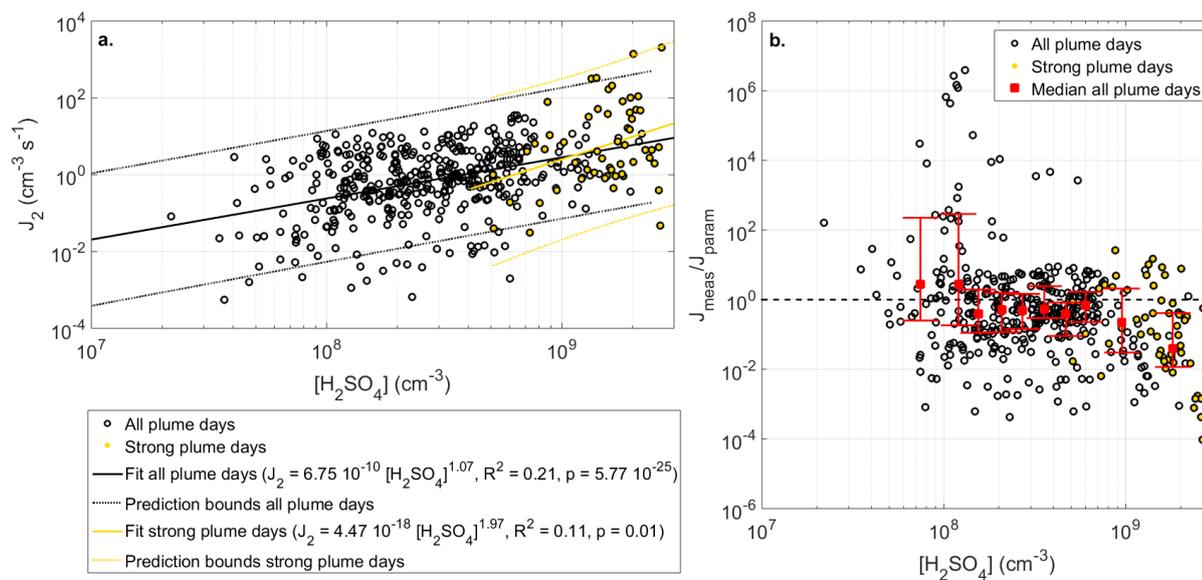
Figure 4 a. Correlation between the formation rate of 2 nm particles (J_2) and [H_2SO_4] on plume days. A power fit was performed on all available datapoints, as well as on those collected on strong plume days separately. b. Ratio between the 2 nm particle formation rates derived from DMPS measurements (J_{meas}) and those describing binary nucleation of $H_2SO_4 – H_2O$ (J_{param}) (Määttänen et al., 2018) as a function of [H_2SO_4]. Data was also binned with respect to [H_2SO_4] (10 bins with equal number of points), and the medians (squares) as well as the 25th/75th percentiles (error bars) of the ratio in each bin are presented. Strong plume days are highlighted with specific markers.
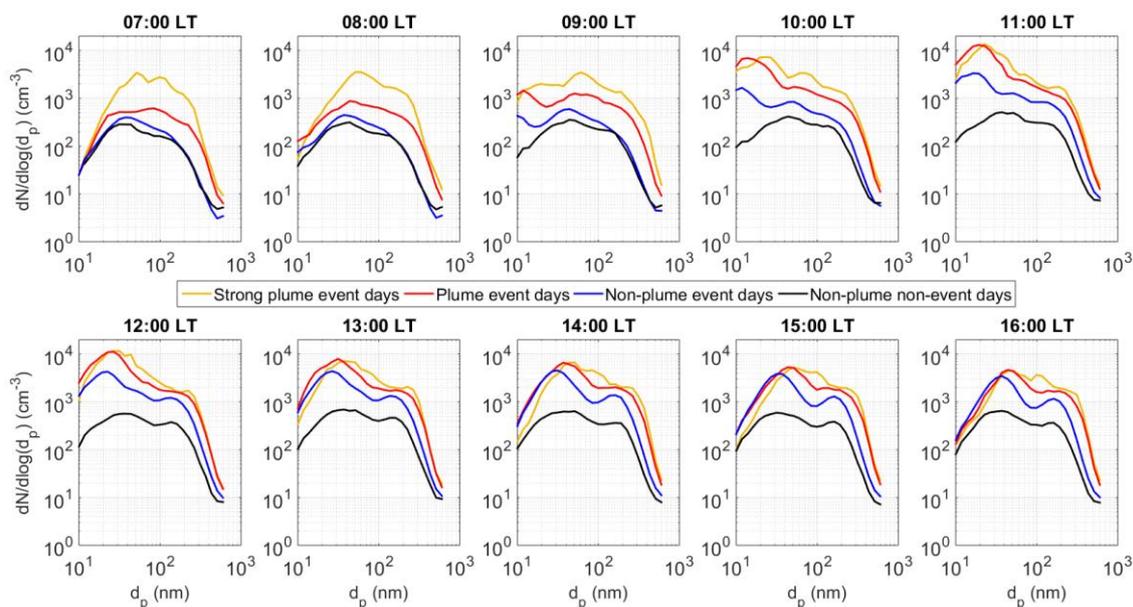
Figure 5 Hourly medians of the particle size distribution derived from DMPS measurements conducted in the different conditions (non-plume NPF event and non-event days, plume and strong plume NPF event days) between 07:00 and 16:00 LT. Note that strong plume days are included in the statistics calculated for plume days, and are also highlighted separately.
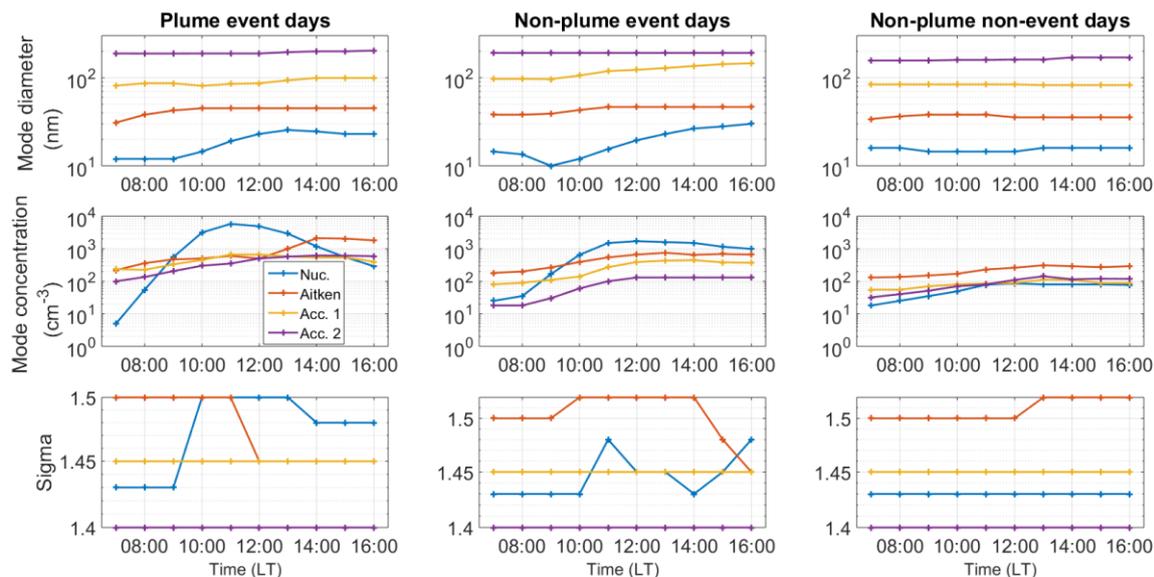
Figure 6 Variations of the parameters of the Gaussians used to fit the hourly median DMPS size distributions shown on Fig. 5. Note that strong plume days are included in the analysis conducted for plume days, but were not fitted separately. All the displayed values are also reported in Table B1 of Appendix B.
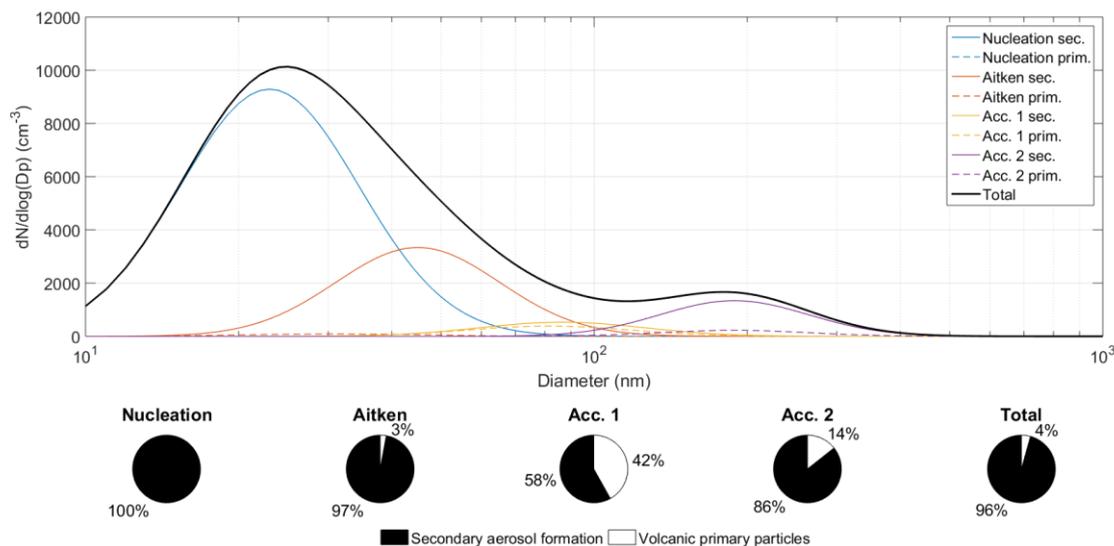
Figure 7 Size distribution of the particles of volcanic origin reconstructed using the spectra measured on plume and non-plume event days. The contributions of primary (i.e. formed/transformed *via* heterogeneous processes in the very close proximity of the vent) and secondary aerosols are shown separately for each mode on the spectrum and are further highlighted on the pie charts.
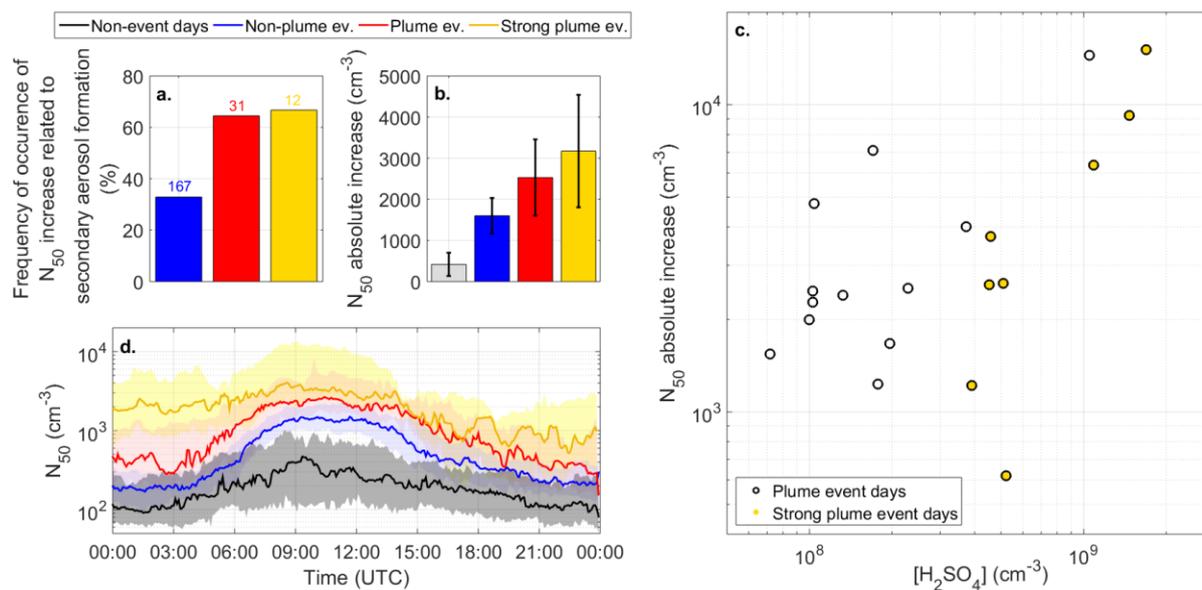
Figure 8 Increase of potential > 50 nm CCN particle concentration (N_{50}) during NPF in and off-plume conditions. a. Frequency of occurrence and b. magnitude of the absolute increase. Note that strong plume days are included in the statistics reported for plume days and are also highlighted separately. See Fig. 2 for an explanation of symbols. In a., numbers on the plot indicate, for non-plume, plume and strong plume conditions, the total number of NPF events included in the statistics. c. Link between the increase of N_{50} and $[H_2SO_4]$ on plume days. Strong plume days are highlighted with specific markers. d. Median diurnal variation of N_{50} in the different conditions, including non-plume non-event days. Lower and upper limits of the shaded areas indicate the 25th and 75th percentiles of the data, respectively.

Appendix A
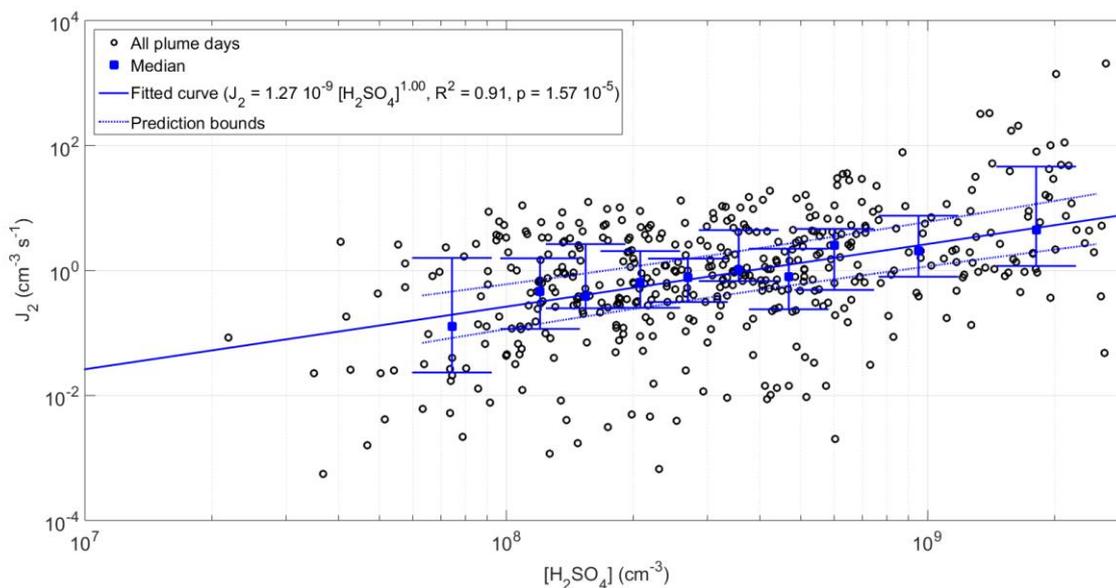
Figure A1 Correlation between the formation rate of 2 nm particles (J_2) and [H2SO4]. Data was binned with respect to [H2SO4] (10 bins with equal number of points), and the medians (squares) as well as the 25th/75th percentiles (error bars) of J_2 in each bin are presented. The power fit was performed on the median values.

Table A1 Effect of the number of bins on both the parameters and goodness of the power fit performed to evaluate the correlation between the formation rate of 2 nm particles (J_2) and [H2SO4], as illustrated on Fi. A1.

Number of bins used in the fitting procedure	k	a	R²	p value
10	1.27×10^{-9}	1.00	0.91	1.57×10^{-5}
20	1.10×10^{-9}	1.05	0.74	1.17×10^{-6}
30	4.48×10^{-10}	1.09	0.72	2.78×10^{-9}

Appendix B

Table B1 Parameters of the Gaussians used to fit the hourly median DMPS size distributions shown on Fig. 5.

Type of days	Time (LT)	Nucleation mode			Aitken mode			1st accumulation mode			2nd accumulation mode		
		N (cm⁻³)	Sigma	d_p (nm)	N (cm⁻³)	Sigma	d_p (nm)	N (cm⁻³)	Sigma	d_p (nm)	N (cm⁻³)	Sigma	d_p (nm)
Plume event days	07:00	5	1,43	12,0	220	1,5	31,0	235	1,45	81,5	100	1,4	188,5
	08:00	55	1,43	12,0	360	1,5	38,0	225	1,45	86,5	135	1,4	188,0
	09:00	550	1,43	12,0	470	1,5	42,5	330	1,45	86,5	205	1,4	188,0
	10:00	3150	1,5	14,5	500	1,5	45,0	450	1,45	81,0	300	1,4	188,5
	11:00	5800	1,5	19,0	600	1,5	45,0	660	1,45	85,0	350	1,4	188,5
	12:00	4900	1,5	23,0	500	1,45	45,0	660	1,45	86,5	500	1,4	188,5
	13:00	2900	1,5	25,5	1000	1,45	45,0	580	1,45	93,5	570	1,4	195,0
	14:00	1180	1,48	24,5	2100	1,45	45,0	540	1,45	99,5	620	1,4	199,5
	15:00	550	1,48	23,0	2050	1,45	45,0	540	1,45	99,5	610	1,4	199,5
	16:00	290	1,48	23,0	1800	1,45	45,0	400	1,45	99,5	590	1,4	203,5
Non-plume event days	07:00	25	1,43	14,5	180	1,5	38,0	80	1,45	97,0	18	1,4	191,0
	08:00	35	1,43	13,5	200	1,5	38,0	90	1,45	97,0	18	1,4	191,0
	09:00	165	1,43	10,0	265	1,5	39,0	110	1,45	96,5	30	1,4	191,0
	10:00	650	1,43	12,0	390	1,52	43,0	140	1,45	106,0	60	1,4	191,0
	11:00	1500	1,48	15,5	540	1,52	46,5	270	1,45	119,0	100	1,4	191,0
	12:00	1700	1,45	19,5	660	1,52	46,5	390	1,45	123,0	130	1,4	191,0
	13:00	1600	1,45	23,0	750	1,52	46,5	430	1,45	129,0	130	1,4	191,0
	14:00	1500	1,43	26,5	650	1,52	46,5	445	1,45	136,0	130	1,4	191,0
	15:00	1150	1,45	28,0	690	1,48	46,5	380	1,45	142,5	130	1,4	191,0
	16:00	990	1,48	30,0	660	1,45	46,5	370	1,45	146,0	130	1,4	191,0
Non-plume non-event days	07:00	18	1,43	16,0	130	1,5	34,0	55	1,45	84,0	32	1,4	157,0
	08:00	25	1,43	16,0	135	1,5	36,5	55	1,45	84,0	40	1,4	157,0
	09:00	35	1,43	14,5	150	1,5	38,0	70	1,45	84,0	51	1,4	157,0
	10:00	49	1,43	14,5	170	1,5	38,0	80	1,45	84,0	70	1,4	159,0
	11:00	78	1,43	14,5	230	1,5	38,0	85	1,45	84,0	80	1,4	159,0
	12:00	86	1,43	14,5	260	1,5	35,5	89	1,45	84,0	110	1,4	161,0
	13:00	80	1,43	16,0	310	1,52	35,5	112	1,45	82,5	142	1,4	161,0
	14:00	80	1,43	16,0	290	1,52	35,5	110	1,45	82,5	115	1,4	170,0
	15:00	80	1,43	16,0	270	1,52	35,5	88	1,45	82,5	120	1,4	170,0
	16:00	77	1,43	16,0	290	1,52	35,5	88	1,45	82,5	118	1,4	170,0

Appendix C
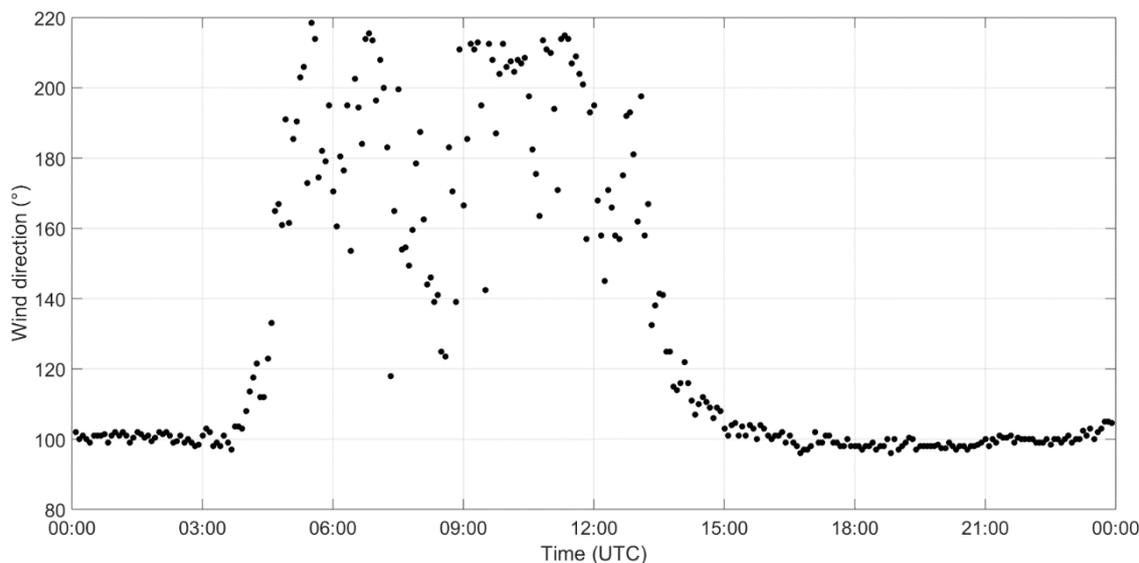
Figure C1 Median diurnal variation of the wind direction measured at Maïdo. All available measurements from 2015 were included in the statistics.

Author contribution

K.S. and P.T. organized the measurements, J.-M.M. conducted the measurements, D.P. contributed to the design of the instrumental setup, C.R., B.F., K.S. and A.C. analysed the data, C.R. and K.S. wrote the manuscript, all authors commented on the manuscript.

Acknowledgements

This work was performed within the framework of H2020 ACTRIS2 (grant agreement No 654109) and ACTRIS-Fr, and has received financial support from the French programme SNO-CLAP. It has also been funded by the OMNCG/OSU-R program from La Réunion University and by the ANR (ANR STRAP, N°ANR-14-CE03-0004-04). We also want to thank ATMO-

15 Réunion for providing SO_2 data.

References

Aiuppa, A., Baker, D. R., and Webster, J. D.: Halogens in volcanic systems, Chemical Geology, 263, 1 – 18, doi:10.1016/j.chemgeo.2008.10.005, 2009.

Albrecht, B. A.: Aerosols, cloud microphysics, and fractional cloudiness, Science, 245(4923), 1227–1230, 1989.

Andres, R. J., and Kasgnoc, A. D.: A time-averaged inventory of subaerial volcanic sulfur emissions, J. Geophys. Res. 103(D19), 25251 - 25261, 1998.

Asmi, E., Freney, E., Hervo, M., Picard, D., Rose, C., Colomb, A., and Sellegri, K.: Aerosol cloud activation in summer and winter at puy-de-Dôme high altitude site in France, Atmos. Chem. Phys., 12, 11589-11607, https://doi.org/10.5194/acp-12-11589-2012, 2012.

Baray, J.-L., Courcoux, Y., Keckhut, P., Portafaix, T., Tulet, P., Cammas, J.-P., Hauchecorne, A., Godin-Beekmann, S., De Mazière, M., Hermans, C. and others: Maïdo observatory: a new high-altitude station facility at Reunion Island (21° S, 55° E) for long-term atmospheric remote sensing and in situ measurements, Atmospheric Meas. Tech., 6(10), 2865–2877, 2013.

Berresheim, H., Adam, M., Monahan, C., O'Dowd, C., Plane, J. M. C., Bohn, B., and Rohrer, F.: Missing SO_2 oxidant in the coastal atmosphere? – observations from high-resolution measurements of OH and atmospheric sulfur compounds, Atmos. Chem. Phys., 14, 12209-12223, https://doi.org/10.5194/acp-14-12209-2014, 2014.

Boulon, J., Sellegri, K., Venzac, H., Picard, D., Weingartner, E., Wehrle, G., Collaud Coen, M., Bütikofer, R., Flückiger, E., Baltensperger, U., and Laj, P.: New particle formation and ultrafine charged aerosol climatology at a high altitude site in the Alps (Jungfraujoch, 3580 m a.s.l., Switzerland), Atmos. Chem. Phys., 10, 9333-9349, https://doi.org/10.5194/acp-10-9333-2010, 2010.

Boulon, J., Sellegri, K., Hervo, M., and Laj, P.: Observations of nucleation of new particles in a volcanic plume, Proc. Natl. Acad. Sci. U.S.A., 108, 12223 – 12226, 2011.

Carslaw, K. S., Lee, L. A., Reddington, C. L., Pringle, K. J., Rap, A., Forster, P. M., Mann, G. W., Spracklen, D. V., Woodhouse, M. T., Regayre, L. A., and Pierce, J. R., Large contribution of natural aerosols to uncertainty in indirect forcing, Nature, 503, 67 – 71, 2013.

Deshler, T., Hofmann, D. J., Johnson, B. J., and Rozier, W. R.: Balloonborne measurements of the Pinatubo aerosol size distribution and volatility at Laramie, Wyoming during the summer of 1991, Geophys. Res. Let., 19(2), 199-202, 1992.

Di Muro, A. , Staudacher, T. , Ferrazzini, V. , Métrich, N. , Besson, P. , Garofalo, C. and Villemant, B. (2015). Shallow Magma Storage at Piton de la Fournaise Volcano After 2007 Summit Caldera Collapse Tracked in Pele's Hairs. In Hawaiian Volcanoes, edited by Carey, R., Cayol, V., Poland, M. and Weis, D., doi:10.1002/9781118872079.ch9, 2015.

Duflot, V., Dils, B., Baray, J. L., De Mazière, M., Attié, J. L., Vanhaelewyn, G., Senten, C., Vigouroux, C., Clain, G., and Delmas, R.: Analysis of the origin of the distribution of CO in the subtropical southern Indian Ocean in 2007, J. Geophys. Res., 115, D22106, doi:10.1029/2010JD013994, 2010.

Foucart, B., Sellegri, K., Tulet, P., Rose, C., Metzger, J.-M., and Picard, D.: High occurrence of new particle formation events at the Maïdo high-altitude observatory (2150 m), Réunion (Indian Ocean), Atmos. Chem. Phys., 18, 9243-9261, https://doi.org/10.5194/acp-18-9243-2018, 2018.

Gordon, H., Sengupta, K., Rap, A., Duplissy, J., Frege, C., Williamson, C., Heinritzi, M., Simon, M., Yan, C., Almeida, J., Tröstl, J., Nieminen, T., Ortega, I. K., Wagner, R., Dunne, E. M., Adamov, A., Amorim, A., Bernhammer, A.-K., Bianchi, F., Breitenlechner, M., Brilke, S., Chen, X., Craven, J. S., Dias, A., Ehrhart, S., Fischer, L., Flagan, R. C., Franchin, A., Fuchs, C., Guida, R., Hakala, J., Hoyle, C. R., Jokinen, T., Junninen, H., Kangasluoma, J., Kim, J., Kirkby, J., Krapf, M., Kürten, A., Laaksonen, A., Lehtipalo, K., Makhmutov, V., Mathot, S., Molteni, U., Monks, V, Onnela, A., Peräkylä, O., Piel, F., Petäjä, T., Praplan, A. P., Pringle, K. J., Richards, N. A. D., Rissanen, M. P., Rondo, L., Sarnela, N., Schobesberger, S., Scott, C. E., Seinfeld, J. H., Sharma, S., Sipilä, M., Steiner, G., Stozhkov, Y., Stratmann, F., Tomé, A., Virtanen, A., Vogel, A. L., Wagner, A. C., Wagner, P. E., Weingartner, E., Wimmer, D., Winkler, P. M., Ye, P., Zhang, X., Hansel, A., Dommen, J., Donahue, N.

M., Worsnop, D. R., Baltensperger, U., Kulmala, M., Curtius, J., and Carslaw, K. S.: Reduced anthropogenic aerosol radiative forcing caused by biogenic new particle formation, Proc. Natl. Acad. Sci. U.S.A., 113, 12053–12058, 2016.

Gordon, H., Kirkby, J., Baltensperger, U., Bianchi, F., Breitenlechner, M., Curtius, J., Dias, A., Dommen, J., Donahue, N., Dunne, E., Duplissy, J., Ehrhart, S., Flagan, R., Ferge, C., Fuchs, C., Hansel, A., Hoyle, C., Kulmala, M., Kürten, A., Lehtipalo, K., Makhmutov, V., Molteni, U., Rissanen, M., Stozhkov, Y., Tröstl, J., Tsagkogeorgas, G., Wagner, R., Williamson, C., Wimmer, D., Winkler, P., Yan, C., and Carslaw, K.: Causes and importance of new particle formation in the present-day and preindustrial atmospheres, J. Geophys. Res.-Atmos., 122, 8739–8760, https://doi.org/10.1002/2017JD026844, 2017.

Hammer, E., Bukowiecki, N., Gysel, M., Jurányi, Z., Hoyle, C. R., Vogt, R., Baltensperger, U., and Weingartner, E.: Investigation of the effective peak supersaturation for liquid-phase clouds at the high-alpine site Jungfraujoch, Switzerland (3580ma.s.l.), Atmos. Chem. Phys., 14, 1123–1139, doi:10.5194/acp-14-11232014, 2014.

Hervo, M., Quennehen, B., Kristiansen, N. I., Boulon, J., Stohl, A., Fréville, P., Pichon, J.-M., Picard, D., Labazuy, P., Gouhier, M., Roger, J.-C., Colomb, A., Schwarzenboeck, A., and Sellegri, K.: Physical and optical properties of 2010 Eyjafjallajökull volcanic eruption aerosol: ground-based, Lidar and airborne measurements in France, Atmos. Chem. Phys., 12, 1721-1736, https://doi.org/10.5194/acp-12-1721-2012, 2012.

Hirsikko, A., Laakso, L., Horrak, U., Aalto, P. P., Kerminen, V. and Kulmala, M.: Annual and size dependent variation of growth rates and ion concentrations in boreal forest, Boreal Environ. Res., 10(5), 357, 2005.

Hirsikko, A., Vakkari, V., Tiitta, P., Manninen, H. E., Gagné, S., Laakso, H., Kulmala, M., Mirme, A., Mirme, S., Mabaso, D., Beukes, J. P. and Laakso, L.: Characterisation of sub-micron particle number concentrations and formation events in the western Bushveld Igneous Complex, South Africa, Atmos. Chem. Phys., 12(9), 3951–3967, doi:10.5194/acp12-3951-2012, 2012.

Jokinen, T., Sipilä, M., Junninen, H., Ehn, M., Lönn, G., Hakala, J., Petäjä, T., Mauldin III, R. L., Kulmala, M., and Worsnop, D. R.: Atmospheric sulphuric acid and neutral cluster measurements using CI-APi-TOF, Atmos. Chem. Phys., 12, 4117-4125, https://doi.org/10.5194/acp-12-4117-2012, 2012.

Junninen, H., Ehn, M., Petäjä, T., Luosujärvi, L., Kotiaho, T., Kostiainen, R., Rohner, U., Gonin, M., Fuhrer, K., Kulmala, M., and Worsnop, D. R.: A high-resolution mass spectrometer to measure atmospheric ion composition, Atmos. Meas. Tech., 3, 1039-1053, https://doi.org/10.5194/amt-3-1039-2010, 2010.

Jurányi, Z., Gysel, M., Weingartner, E., Bukowiecki, N., Kammermann, L., and Baltensperger, U.: A 17 month climatology of the cloud condensation nuclei number concentration at the high alpine site Jungfraujoch, J. Geophys. Res., 116, D10204, doi:10.1029/2010JD015199, 2011.

Kerminen, V.-M., Paramonov, M., Anttila, T., Riipinen, I., Fountoukis, C., Korhonen, H., Asmi, E., Laakso, L., Lihavainen, H., Swietlicki, E., Svenningsson, B., Asmi, A., Pandis, S. N., Kulmala, M., and Petäjä, T.: Cloud condensation nuclei production associated with atmospheric nucleation: a synthesis based on existing literature and new results, Atmos. Chem. Phys., 12, 12037–12059, doi:10.5194/acp-12-12037-2012, 2012.

Kerminen, V.-M., Chen, X., Vakkari, V., Petäjä, T., Kulmala, M., and Bianchi, F.: Atmospheric new particle formation and growth: review of field observations, Environ. Res. Lett., 10, https://doi.org/10.1088/1748-9326/aadf3c, 2018.

Kuang, C., McMurry, P. H., McCormick, A. V. and Eisele, F. L.: Dependence of nucleation rates on sulfuric acid vapor concentration in diverse atmospheric locations, J. Geophys. Res. Atmospheres, 113(D10), https://doi.org/10.1029/2007JD009253, 2008.

Kulmala, M., Lehtinen, K. E. J. and Laaksonen, A.: Cluster activation theory as an explanation of the linear dependence between formation rate of 3nm particles and sulphuric acid concentration, Atmos Chem Phys, 6(3), 787–793, doi:10.5194/acp-6-787-2006, 2006.

Kulmala, M., Petäjä, T., Nieminen, T., Sipilä, M., Manninen, H. E., Lehtipalo, K., Dal Maso, M., Aalto, P. P., Junninen, H., and Paasonen, P.: Measurement of the nucleation of atmospheric aerosol particles, Nat. Protoc., 7, 1651–1667, doi:10.1038/nprot.2012.091, 2012.

Kulmala, M., Kontkanen, J., Junninen, H., Lehtipalo, K., Manninen, H. E., Nieminen, T., Petäjä, T., Sipilä, M., Schobesberger, S., Rantala, P., Franchin, A., Jokinen, T., Järvinen, E., Äijälä, M., Kangasluoma, J., Hakala, J., Aalto, P. P., Paasonen, P., Mikkilä, J., Vanhanen, J., Aalto, J., Hakola, H., Makkonen, U., Ruuskanen, T., Mauldin, R. L., Duplissy, J., Vehkamäki, H., Bäck, J., Kortelainen, A., Riipinen, I., Kurtén, T., Johnston, M. V., Smith, J. N., Ehn, M., Mentel, T. F., Lehtinen, K. E. J., Laaksonen, A., Kerminen, V.-M. and Worsnop, D. R.: Direct Observations of Atmospheric Aerosol Nucleation, Science, 339(6122), 943–946, doi:10.1126/science.1227385, 2013.

Lehtinen, K. E. J., Dal Maso, M., Kulmala, M. and Kerminen, V.-M.: Estimating nucleation rates from apparent particle formation rates and vice versa: Revised formulation of the Kerminen–Kulmala equation, J. Aerosol Sci., 38(9), 988–994, doi:10.1016/j.jaerosci.2007.06.009, 2007.

Määttänen, A., Merikanto, J., Henschel, H., Duplissy, J., Makkonen, R., Ortega, I. K., and Vehkamäki, H.: New parameterizations for neutral and ion-induced sulfuric acid – water particle formation in nucleation and kinetic regimes, J. Geophys. Res., 123, 1269 – 1296, https://doi.org/10.1002/2017JD027429, 2018.

Makkonen, R., Asmi, A., Kerminen, V.-M., Boy, M., Arneth, A., Hari, P., and Kulmala, M.: Air pollution control and decreasing new particle formation lead to strong climate warming, Atmos. Chem. Phys., 12, 1515–1524, doi:10.5194/acp-12-15152012, 2012.

Mallik, C., Ghosh, D., Ghosh, D., Sarkar, U., Lal, S., and Venkataramani, S.: Variability of SO2, CO, and light hydrocarbons over a megacity in Eastern India: effects of emissions and transport, Environ. Sci. Pollut. Res., 21(14), 8692-8706, https://doi.org/10.1007/s11356-014-2795-x, 2014.

Mather, T. A.: Volcanoes and the environment: Lessons for understanding Earth's past and future from studies of present-day volcanic emissions, Journal of Volcanology and Geothermal Research, 304, 160-179, 2015.

Mauldin III, R. L., Cantrell, C. A., Zondlo, M., Kosciuch, E., Eisele, F. L., Chen, G., Davis, D., Weber, R., Crawford, J., Blake, D., Bandy, A., and Thornton, D.: Highlights of OH, H2SO4, and methane sulfonic acid measurements made aboard the NASA P-3B during Transport and Chemical Evolution over the Pacific, J. Geophys. Res., 108(D20), 8796, doi:10.1029/2003JD003410, 2003.

Merikanto, J., Spracklen, D. V., Mann, G. W., Pickering, S. J., and Carslaw, K. S.: Impact of nucleation on global CCN, Atmos. Chem. Phys., 9, 8601–8616, doi:10.5194/acp-9-8601-2009, 2009.

Mikkonen, S., Romakkaniemi, S., Smith, J. N., Korhonen, H., Petäjä, T., Plass-Duelmer, C., Boy, M., McMurry, P. H., Lehtinen, K. E. J., Joutsensaari, J., Hamed, A., Mauldin III, R. L., Birmili, W., Spindler, G., Arnold, F., Kulmala, M., and Laaksonen, A.: A statistical proxy for sulphuric acid concentration, Atmos. Chem. Phys., 11, 11319–11334, doi:10.5194/acp-11-11319-2011, 2011.

Mirme, A., Tamm, E., Mordas, G., Vana, M., Uin, J., Mirme, S., Bernotas, T., Laakso, L., Hirsikko, A. and Kulmala, M.: A widerange multi-channel Air Ion Spectrometer, Boreal Environ. Res., 12(3), 247–264, 2007.

Myhre, G., Shindell, D., Bréon, F.-M., Collins, W., Fuglestvedt, J., Huang, J., Koch, D., Lamarque, J.-F., Lee, D., Mendoza, B., Nakajima, T., Robock, A., Stephens, G., Takemura, T., and Zhang, H.: Anthropogenic and Natural Radiative Forcing, Contribution of Working Group I to the Fifth Assessment Report of the Intergovernmental Panel on Climate Change, edited by Stocker, T.F., Qin, D., Plattner, G.-K., Tignor, M., Allen, S.K., Boschung, J., Nauels, A., Xia, Y., Bex, V., and Midgley, P.M., Cambridge University Press, Cambridge, United Kingdom and New York, NY, USA, 2013.

Penner, J.E., Andreae, M., Annegarn, H., Barrie, L., Feichter, J., Hegg, D., Jayaraman, A., Leaitch, R., Murphy, D., Nganga, J., and Pitari, G.: Aerosols, their direct and indirect effects, Contribution of Working Group I to the Third Assessment Report of the Intergovernmental Panel on Climate Change, edited by B. Nyenzi, B., and Prospero, J., Cambridge University Press, Cambridge, United Kingdom and New York, NY, USA, 2001.

Petäjä, T., Mauldin, III, R. L., Kosciuch, E., McGrath, J., Nieminen, T., Paasonen, P., Boy, M., Adamov, A., Kotiaho, T., and Kulmala, M.: Sulfuric acid and OH concentrations in a boreal forest site, Atmos. Chem. Phys., 9, 7435–7448, doi:10.5194/acp9-7435-2009, 2009.

Roberts, G. C. and Nenes, A.: A continuous-flow streamwise thermal-gradient CCN chamber for atmospheric measurements, Aerosol Sci. Technol., 39, 206–221, 2005.

Robock, A.: Volcanic eruptions and climate, Reviews of Geophysics, 38, 191 – 219, 2000.

Rose, C., Boulon, J., Hervo, M., Holmgren, H., Asmi, E., Ramonet, M., Laj, P., and Sellegri, K.: Long-term observations of cluster ion concentration, sources and sinks in clear sky conditions at the high-altitude site of the Puy de Dôme, France, Atmos. Chem. Phys., 13, 11573-11594, https://doi.org/10.5194/acp-13-11573-2013, 2013.

Rose, C., Sellegri, K., Velarde, F., Moreno, I., Ramonet, M., Weinhold, K., Krejci, R., Andrade, M., Wiedensohler, A., and Laj, P.: Frequent nucleation events at the high-altitude station of Chacaltaya (5240ma.s.l.), Bolivia, Atmos. Environ., 102, 18–29, doi:10.1016/j.atmosenv.2014.11.015, 2015.

Rose, C., Sellegri, K., Moreno, I., Velarde, F., Ramonet, M., Weinhold, K., Krejci, R., Andrade, M., Wiedensohler, A., Ginot, P., and Laj, P.: CCN production by new particle formation in the free troposphere, Atmos. Chem. Phys., 17, 1529-1541, https://doi.org/10.5194/acp-17-1529-2017, 2017.

Rosenfeld, D., Sherwood, S., Wood, R. and Donner, L.: Climate Effects of Aerosol Cloud Interactions, Science, 343(6169), 379–380, doi:10.1126/science.1247490, 2014.

Schmidt, A., Carslaw, K. S., Mann, G. W., Rap, A., Pringle, K. J., Spracklen, D. V., Wilson, M., and Forster, P. M.: Importance of tropospheric volcanic aerosol for indirect radiative forcing of climate, Atmos. Chem. Phys., 12, 7321-7339, https://doi.org/10.5194/acp-12-7321-2012, 2012.

Seinfeld, J.H. and Pandis, S.N.: Atmospheric Chemistry and Physics: From Air Pollution to Climate Change, 2nd Edition, John Wiley & Sons, New York, 2006.

Sihto, S.-L., Kulmala, M., Kerminen, V.-M., Dal Maso, M., Petäjä, T., Riipinen, I., Korhonen, H., Arnold, F., Janson, R., Boy, M., Laaksonen, A. and Lehtinen, K. E. J.: Atmospheric sulphuric acid and aerosol formation: implications from atmospheric measurements for nucleation and early growth mechanisms, Atmos Chem Phys, 6(12), 4079–4091, doi:10.5194/acp-6-40792006, 2006.

Sipilä, M., Berndt, T., Petäjä, T., Brus, D., Vanhanen, J., Stratmann, F., Patokoski, J., Mauldin, R. L., Hyvärinen, A.-P., Lihavainen, H. and Kulmala, M.: The Role of Sulfuric Acid in Atmospheric Nucleation, Science, 327(5970), 1243–1246, doi:10.1126/science.1180315, 2010.

Sipilä, M., Sarnela, N., Jokinen, T., Henschel, H., Junninen, H., Kontkanen, J., Richters, S., Kangasluoma, J., Franchin, A., Peräkylä, O., Rissanen, M. P., Ehn, M., Vehkamäki, H., Kurten, T., Berndt, T., Petäjä, T., Worsnop, D., Ceburnis, D., Kerminen, V.-M., Kulmala, M., and O'Dowd, C.: Molecular-scale evidence of aerosol particle formation via sequential addition of HIO3, Nature, 537, 532-534, doi:10.1038/nature19314, 2016.

5 Tröstl, J., Herrmann, E., Frege, C., Bianchi, F., Molteni, U., Bukowiecki, N., Hoyle, C. R., Steinbacher, M., Weingartner, E., Dommen, J., Gysel, M., and Baltensperger, U.: Contribution of new particle formation to the total aerosol concentration at the high altitude site Jungfraujoch (3580ma.s.l., Switzerland), J. Geophys. Res.-Atmos., 121, 11692–11711, doi:10.1002/2015JD024637, 2016.

Tulet, P., Di Muro, A., Colomb, A., Denjean, C., Duflot, V., Arellano, S., Foucart, B., Brioude, J., Sellegri, K., Peltier, A.,
10 Aiuppa, A., Barthe, C., Bhugwant, C., Bielli, S., Boissier, P., Boudoire, G., Bourrianne, T., Brunet, C., Burnet, F., Cammas, J.-P., Gabarrot, F., Galle, B., Giudice, G., Guadagno, C., Jeamblu, F., Kowalski, P., Leclair de Bellevue, J., Marquestaut, N., Mékies, D., Metzger, J.-M., Pianezze, J., Portafaix, T., Sciare, J., Tournigand, A., and Villeneuve, N.: First results of the Piton de la Fournaise STRAP 2015 experiment: multidisciplinary tracking of a volcanic gas and aerosol plume, Atmos. Chem. Phys., 17, 5355-5378, https://doi.org/10.5194/acp-17-5355-2017, 2017.

15 Vakkari, V., Laakso, H., Kulmala, M., Laaksonen, A., Mabaso, D., Molefe, M., Kgabi, N., and Laakso, L.: New particle formation events in semi-clean South African savannah, Atmos. Chem. Phys., 11, 3333-3346, https://doi.org/10.5194/acp-11-3333-2011, 2011.

Vanhanen, J., Mikkilä, J., Lehtipalo, K., Sipilä, M., Manninen, H. E., Siivola, E., Petäjä, T. and Kulmala, M.: Particle Size Magnifier for Nano-CN Detection, Aerosol Sci. Technol., 45(4), 533–542, doi:10.1080/02786826.2010.547889, 2011.

20 Venzac, H., Sellegri, K., Laj, P., Villani, P., Bonasoni, P., Marinoni, A., Cristofanelli, P., Calzolari, F., Fuzzi, S. and Decesari, S.: High frequency new particle formation in the Himalayas, Proc. Natl. Acad. Sci., 105(41), 15666–15671, 2008.

Vigouroux, C., Stavrakou, T., Whaley, C., Dils, B., Duflot, V., Hermans, C., Kumps, N., Metzger, J.-M., Scolas, F., Vanhaelewyn, G., Müller, J.-F., Jones, D. B. A., Li, Q., and De Mazière, M.: FTIR time-series of biomass burning products (HCN, C2H6, C2H2, CH3OH, and HCOOH) at Reunion Island (21° S, 55° E) and comparisons with model data, Atmos. Chem.
25 Phys., 12, 10367-10385, https://doi.org/10.5194/acp-12-10367-2012, 2012.

Wiedensohler, A., Birmili, W., Nowak, A., Sonntag, A., Weinhold, K., Merkel, M., Wehner, B., Tuch, T., Pfeifer, S., Fiebig, M., Fjäraa, A. M., Asmi, E., Sellegri, K., Depuy, R., Venzac, H., Villani, P., Laj, P., Aalto, P., Ogren, J. A., Swietlicki, E., Williams, P., Roldin, P., Quincey, P., Hüglin, C., FierzSchmidhauser, R., Gysel, M., Weingartner, E., Riccobono, F., Santos, S., Grüning, C., Faloon, K., Beddows, D., Harrison, R., Monahan, C., Jennings, S. G., O'Dowd, C. D., Marinoni, A., Horn,
30 H.-G., Keck, L., Jiang, J., Scheckman, J., Mcmurry, P. H., Deng, Z., Zhao, C. S., Moerman, M., Henzing, B., De Leeuw, G., Löschau, G. and Bastian, S.: Mobility particle size spectrometers: harmonization of technical standards and data structure to facilitate high quality long-term observations of atmospheric particle number size distributions, Atmospheric Meas. Tech., 5, 657–685, doi:10.5194/amt-5-657-2012, 2012.

Yan, C., Dada, L., Rose, C., Jokinen, T., Nie, W., Schobesberger, S., Junninen, H., Lehtipalo, K., Sarnela, N., Makkonen, U.,
35 Garmash, O., Wang, Y., Zha, Q., Paasonen, P., Bianchi, F., Sipilä, M., Ehn, M., Petäjä, T., Kerminen, V.-M., Worsnop, D. R., and Kulmala, M.: The role of H2SO4-NH3 anion clusters in ion-induced aerosol nucleation mechanisms in the boreal forest, Atmos. Chem. Phys., 18, 13231-13243, https://doi.org/10.5194/acp-18-13231-2018, 2018.

Zelenski, M., Taran, Y., and Galle, B.: High emission rate of sulfuric acid from Bezymianny volcano, Kamchatka, Geophys. Res. Lett., 42, 7005–7013, doi:10.1002/2015GL065340, 2015.
40